Muddy sediments are an important potential source of silicon in coastal and continental margin zones

Muddy Sediments are an Important Potential Source of Silicon in Coastal and Continental Margin Zones

Dongdong Zhu[1,2,3], Su Mei Liu[1,2]*, Aude Leynaert[3], Paul Tréguer[3], Jingling Ren[1,2], Jonas Schoelynck[4], Yuwei Ma[1,2], Jill N. Sutton[3]*

[1]Frontiers Science Center for Deep Ocean Multi-spheres and Earth System, Key Laboratory of Marine Chemistry Theory and Technology, Ministry of Education, Ocean University of China, Qingdao, China

[2]Laboratory for Marine Ecology and Environmental Science, Qingdao National Laboratory for Marine Science and Technology, Qingdao, China

[3]University of Brest, Centre national de la recherche scientifique, Institut de recherche pour le développement, Ifremer, Institut Universitaire Européen de la Mer, Plouzané, France

[4]Department of Biology, Ecosphere Research Group, University of Antwerp, Universiteitsplein 1, Wilrijk, Belgium

* Correspondences:

Dr. Su Mei Liu, Email : sumeiliu@ouc.edu.cn

Address : No.238 Songling Road, Laoshan District, 266100 Qingdao, China

Dr. Jill N. Sutton, Email: jill.sutton@univ-brest.fr

Address: Rue Dumont d'Urville, 29280 Plouzané, France

Abstract

The dissolution of silicate minerals on the seafloor releases an important amount of dissolved silicon (dSi), which is necessary for maintaining high diatom production in Coastal and Continental Margin Zones (CCMZs). However, the dissolution of silicate minerals along the continental shelves is variable, which hinders our understanding of the marine Si cycle on both a regional and global scale. To understand the discrepancy of silicon (Si) released in different sediment matrices and its potential controlling factors, we investigated surface sediments of typical CCMZs of the Chinese marginal Seas using a continuous alkaline extraction technique, grain size and chemical (carbon and total nitrogen) analysis as well as a qualitative measurement of clay mineral composition by X-ray diffraction. The results showed that the amount of Si and aluminum (Al) leached from muddy sediments were 2 times greater than those released from sandy sediments. High dissolution rates (> 0.20 mg-SiO_2 g^{-1} min^{-1}) of silicate minerals are caused by a large sediment-specific surface area. Further, our data showed that biogenic silica (bSi) with high Al content (Si:Al < 40) has low reactivity and that the source of Al incorporated in bSi is silicate minerals undergoing dissolution. We show that although the dissolution of silicate minerals is less active than that of bSi, it still potentially releases more bio-available Si and Al to seawater due to its dominant presence on the seafloor (70.3% − 99.0%wt). This study highlights silicate minerals as an important potential marine Si source and emphasizes the need for a better understanding of the roles of silicate minerals in the Si cycle of marginal seas in future studies.

Graphical Abstract:

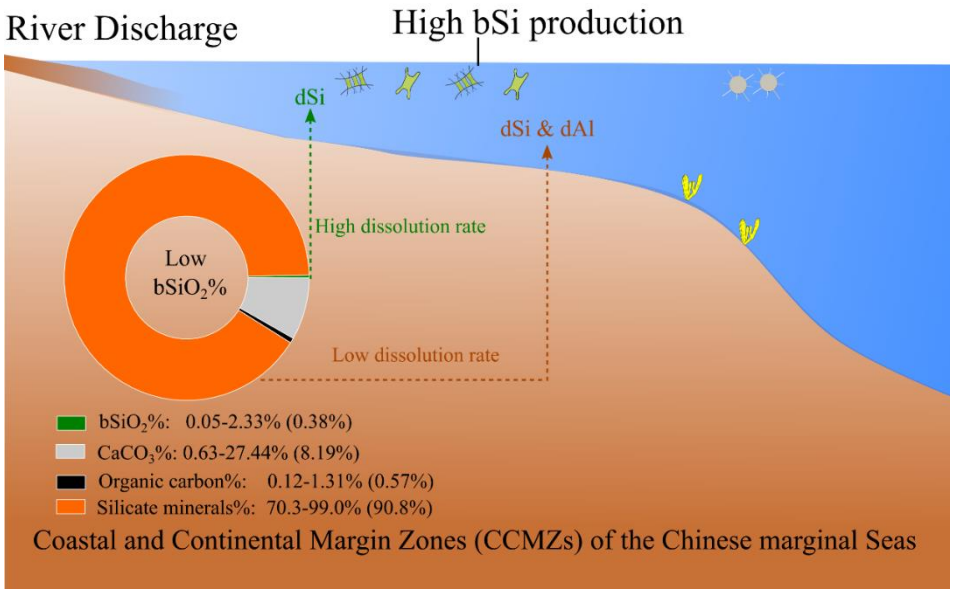

Highlights:

- Muddy sediments potentially release two times more Si and Al than sandy sediments.
- Elevated values of alkaline extracted Si and Al are due to a large sediment-specific surface area.
- Reactivity of biogenic silica in sediments is reduced because of the incorporated Al that originates from silicate minerals.
- Models show that Si:Al ratios of the linearly dissolving lithogenic silicate phases are correlated with the major types of clay minerals in sediments.

Keywords: Continuous Alkaline Extraction; Silicate Dissolution; Silicon Cycle; Coastal and Continental Margin Zones

1. Introduction

Riverine discharge is the main external marine silicon (Si) source to Coastal and Continental Margin Zones (CCMZs) (Tréguer et al., 2021). As a consequence of climate change, a decrease in riverine dissolved Si (dSi) discharge (Phillips, 2020) to the oceans is expected. Moreover, with a warmer and more stratified ocean, there will be lower nutrient input from depth, leading to lower diatom production and resulting in a decline in biogenic silica (bSi) export in mid and low-latitude oceans (Tréguer et al., 2018). Alternatively, Taucher et al. (2022) predicted that with ocean acidification, the pH-induced decrease in bSi dissolution will reduce the availability of silicic acid in the surface ocean, consequently triggering a global diatom decline. The dissolution of silicate minerals in sediments of CCMZs contributes an important amount of dSi (ranging from 2 to 45 Tmol-Si yr^{-1}) to the global ocean (Jeandel et al., 2011; Jeandel and Oelkers, 2015; Frings, 2017; Tréguer et al., 2021), which fuels planktonic and benthic diatom production (Tréguer et al., 1995; Leynaert et al., 2011). Jeandel et al. (2011) and Jeandel (2016) highlighted the importance of silicate mineral dissolution in the silicate-rich CCMZs as a necessary Si source of the oceans. Given the importance of silicate minerals dissolution for supplying Si to the ocean and sustaining oceanic productivity (Fabre et al., 2019; Zhang et al., 2020; Measures and Hatta, 2021; Ng et al., 2020, 2022; Ward et al., 2022), understanding the variability of silicate mineral dissolution along continental margins (Lerman et al., 1975; Jeandel et al., 2011; Jeandel and Oelkers, 2015) and evaluating its Si-release potential are necessary (Barão et al., 2015).

The interaction of silicate minerals with seawater contributes to the control of the dSi concentration of seawater, with silicate minerals releasing Si to the silica-deficient seawater and precipitating Si from silicic acid enriched (> 417 μM) seawater (Mackenzie et al., 1967; Siever, 1968). Based on theoretical and empirical studies of porewater dSi profiles, Frings (2017) concluded that 45 Tmol-Si yr^{-1} is released from clay and calcareous seafloor. However, Tréguer et al. (2021) found that some of the non-biogenic-silica sediment classes described in Frings (2017) contain significant bSi,

which explains the overestimation of the benthic Si efflux. The re-evaluated benthic Si efflux from opal-poor sediments is approximately 2 Tmol-Si yr^{-1}, which still represents 13% of the total marine Si input (Tréguer et al., 2021). Quantitatively differentiating the Si outflux of silicate minerals from bSi is challenging due to complex mineral compositions (Jeandel et al., 2011; Tréguer et al., 2021). A flow-through experiment was established for evaluating the Si efflux from bulk sediment of various depositional environments (Open Ocean (Van Cappellen and Qiu, 1997; Rickert, 2000; Gallinari et al., 2002, 2008) and CCMZs (Wu et al., 2017; Wu and Liu, 2020; Ma et al., 2023)). However, the Si released during the flow-through experiment originates from both bSi and silicate minerals, and the relative contribution of either Si source is not distinguished according to the measurement of dSi concentrations only (Ma et al., 2023). In this study, we use a simultaneous measurement of dSi and dissolved aluminum (dAl) in order to address this issue (Kamatani and Oku, 2000; Koning et al., 2002), since the Al content in bio-siliceous frustules is far less than in mineral sediments (Ehlert et al., 2012).

The continuous alkaline extraction technique is an advanced wet chemical method that simultaneously analyzes dSi and dAl (Koning et al., 2002) and is widely applied for differentiating different sources of Si from soil (Barão et al., 2014, 2015) and marine sediments (Koning et al., 2002; Barão et al., 2015; Raimonet et al., 2015; Zhu et al., 2023). Through a high-resolution (one-second) alkaline extraction monitoring of the dSi and dAl contents and a first-order dissolution model, sources of Si are well-defined based on the different dissolution kinetics and elemental compositions of bSi and silicate minerals (i.e., lithogenic silica) (Koning et al., 2002). This technique allows accurate quantification of the bSi content (bSi%) and the lithogenic silica content, particularly for sediments of CCMZs where silicate mineral content far exceeds the bSi% (Barão et al., 2015; Zhu et al., 2023). Previous studies found that the amount of alkaline-extracted Si from silicate minerals is significantly higher than bSi (Barão et al., 2015). Although silicate mineral digestion, performed in the laboratory, is significantly enhanced under the hot (85 °C) conditions of alkaline digestion, it suggests the potential importance of non-biogenic silicate as a source of silicate for marine ecosystems (Barão

et al, 2015). Further, in situ measurement of the dissolution rate of aluminosilicates in seawater was found to be comparable to the dissolution of bSi in oceanic sediments, particularly for silicate minerals of surface sediments that contain highly active surface areas (Lerman et al., 1975; Köhler et al., 2005). This is probably due to 1) reduced dissolution rate of bSi caused by authigenic aluminosilicate coating surrounding the bio-siliceous structures (Michalopoulos and Aller, 1995, 2004; Michalopoulos et al., 2000; Amann et al., 2020) and 2) relative rapid dissolution of silicate minerals in surface sediments (Köhler et al., 2005). Therefore, simultaneous alkaline extractions can help quantify different Si fractions that are more soluble than the highly crystalized minerals and can be released back into seawater.

CCMZs are "boundary exchange zones" that play a major role in the land-to-ocean transfer of materials (Jeandel and Oelkers, 2015). As the largest CCMZs in western Pacific, the Chinese marginal Seas (i.e., the Bohai Sea (BH), Yellow Sea (YS), East China Sea (ECS) and South China Sea (SCS)) receive more than 1.4×10^9 tons yr^{-1} of terrestrial sediments from surrounding rivers (Milliman and Meade, 1983; Liu et al., 2009; Qiao et al., 2017; Ma et al., 2022). Even a lower limit of dissolution rate (0.5%-SiO_2 yr^{-1}, Jeandel et al., 2011; Jeandel and Oelkers, 2015) of the riverine transported solid phases would release 1.2×10^{11} mol-Si yr^{-1} into the marine water column, which is still comparable to the dSi input from all surrounding rivers (6.4×10^{11} mol-Si yr^{-1}, (Liu et al., 2003, 2005, 2009, 2011). In addition, both field observations and onboard/laboratory incubations have shown that the Si efflux from the opal-poor sediments plays a major role in the diatom production of the BH (Liu et al., 2011), YS (Liu et al., 2003; Wu et al., 2017), ECS (Wu and Liu, 2020) and SCS (Ma et al., 2022), as well as other CCMZs (i.e., the southern North Sea, Gehlen and van Raaphorst, 1993; Oehler et al., 2015). It is therefore important to understand the role of bSi and silicate minerals dissolutions in Si efflux and more broadly, in the biogeochemical cycle of Si in the CCMZs.

In this context, we measured the chemical compositions (i.e., total organic carbon, inorganic carbon, total nitrogen), physical properties (i.e., grain size) and the clay mineral contents of sediments to understand the sediment matrices. We conducted

continuous alkaline extraction experiments to simultaneously monitor the dissolution of bSi and silicate minerals in sediments, and further quantified the amount of different Si phases (bSi and silicate minerals) released from various types of sediments (muddy vs. sandy sediments) collected in the CCMZs of the Chinese marginal Seas.

2. Materials and Methods

2.1. Sampling of Sediment Samples

Surface sediments (0 − 2 cm) were collected from the BH, YS, ECS and SCS during August − September 2008, September − October 2010, May − June 2013 and March − April 2014, respectively (Figure 1). Information (research cruise, date, samples' coordinates and water depth) of these samples is described in Wu et al, (2017), Ma et al, (2023) and Zhu et al, (2023). All samples were sealed in plastic bags and immediately stored on board at -20 ℃ and freeze-dried in the laboratory for further analysis.

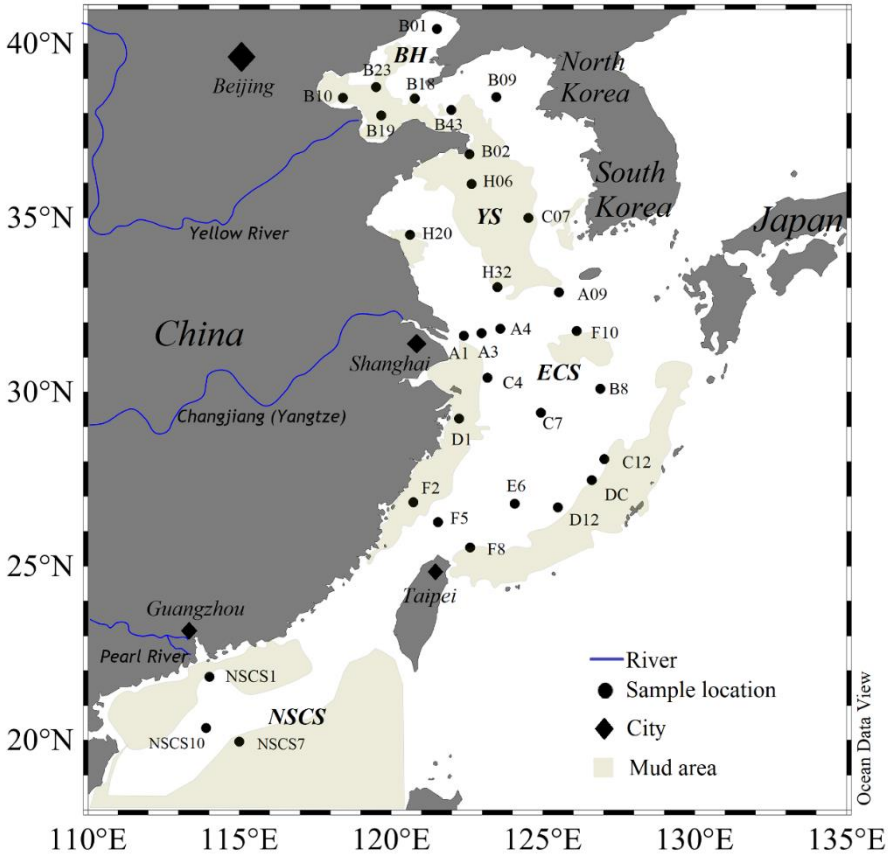

Figure 1. Map of the Chinese marginal Seas showing sampling stations in the Bohai

Sea (BH), Yellow Sea (YS), East China Sea (ECS) and northern South China Sea (NSCS). Mud deposits are also indicated following Wu and Wen (2019) and Shi et al. (2021). Figure plotted using Ocean Data View (ODV) program (Schlitzer, 2023).

2.2. Analytical Methods

2.2.1 Continuous Alkaline Extractions

The simultaneous alkaline extraction of Si and Al was conducted following the wet chemical method described in previous studies (Koning et al., 2002; Barão et al., 2015; Zhu et al., 2023). The high-resolution analysis (one second) of alkaline extracted dSi and dAl allows 1) an evaluation of the alkaline extracted Si fractions from bSi and silicate minerals, as the Al content of diatoms in sediments is less than that of silicate minerals (Koning et al., 2002; Ehlert et al., 2012), and 2) the determination of the dissolution kinetics of bSi and silicate minerals. In brief, freeze-dried sediments were added into a stainless-steel vessel filled with 180 mL of 0.5 M NaOH pre-heated to 85℃. The alkaline extracted Si concentration was measured according to the molybdate-blue method (Grasshoff et al., 1983) and the Al concentration was determined according to the fluorometric method (Hydes and Liss, 1976). Standard samples of dSi and dAl with concentrations of 1 mg L^{-1}, 2 mg L^{-1}, 4 mg L^{-1}, 6 mg L^{-1}, 8 mg L^{-1}, 10 mg L^{-1}, 20 mg L^{-1}, 30 mg L^{-1}, and 40 mg L^{-1} were used for calibration, and only the linear regression curves with correlation coefficients ≥ 0.999 were accepted according to previous studies (Barão et al., 2015). Two independent internal reference solutions (with concentrations of 3 mg L^{-1}, and 9 mg L^{-1} of dSi and dAl) were tested before and after the continuous alkaline extractions to guarantee an analytical error below 5%. Triplicate analyses of sample C12 were conducted, and the standard deviation for three parallel extractions was < 3%, indicating good reproducibility (Zhu et al., 2023). The concentrations of dSi and dAl of the reagents blank solutions were at the baseline of measurements. Samples from the BH, YS and ECS were digested previously, and the modeling parameters were reported in Zhu et al. (2023), three samples (NSCS1, NSCS7 and NSCS10) from the SCS were analyzed in this study. The period of alkaline extraction ranged from 30 min to 70 min (50 min on average). The

stock solutions for Si and Al concentration analyses were made using $Na_2SiO_3 \cdot 9H_2O$ (Sigma-Aldrich S4392) and $KAl(SO_4)_2 \cdot 12H_2O$ (Merck 101047). The standard solutions and the internal independent reference solutions were prepared by diluting the stock solution.

2.2.2. Analytical Procedure for Si and Al data

Each extraction provides Si and Al concentrations over time, and unit of time t in equation (Eq. 1) was normalized into minutes (min). Calculation of the bSi content (bSi%) follows the procedure that assumes the presence of a linearly dissolving silicate mineral phase and a non-linearly dissolving silica phase indicating bSi and /or non-bSi (Koning et al., 2002).

All alkaline extracted Si and Al concentrations were fitted (Eq.1) using the first-order dissolution models (model 1: i =1; model 2: i =2, model 3: i =3) as described in Koning et al. (2002), Barão et al. (2015) and Zhu et al. (2023). Here, Eq.1 describes sediments containing several non-linearly dissolving Si phases ($ExtrSi_1$, $ExtrSi_2$, $ExtrSi_3$):

$$Si_{aq} = \sum_{i}^{n} [ExtrSi_i]_0 \, (1 - e^{-k_i t}) + bt$$

$$Al_{aq} = \sum_{i}^{n} \frac{1}{\beta_i} [ExtrSi_i]_0 \, (1 - e^{-k_i t}) + \frac{1}{\beta_{lin}} \, bt \qquad (1)$$

Where Si_{aq} and Al_{aq} are the concentrations of leached dSi and dAl in mg L^{-1}, at time t (min). $[ExtrSi_i]_0$ is the initial extractable Si in mg L^{-1}, calculated under a condition when all alkaline extractable Si (bSi and silicate mineral) has dissolved, k_i is the reactivity constant (min^{-1}) of non-linear dissolving phases and β_i is the atomic ratio of Si and Al released during the dissolution of extractable silica fraction. The parameters b and β_{lin} represent the constant dissolution rate and the Si:Al ratios of silicate minerals, respectively. Normally, several alkaline extractable Si ($ExtrSi_i$) phases exist, the bSi phases are characterized by a high Si:Al ratio ($\beta_i > 5$) and high reactivity ($k_i >$ 0.1 min^{-1}) (Koning et al., 2002). Further, the total amount of alkaline extracted Si (TAlkSi, mg-Si g^{-1}) and Al (TAlkAl, mg-Al g^{-1}) were also presented. For the fitted

results from the above-mentioned models (see Eq.1), optimization was carried out by maximizing the likelihood statistic and parameters of the optimum model were adopted. Detailed calculations of the likelihood statistic are provided in Armstrong et al. (2002), Moriceau et al. (2009) and Zhu et al. (2023). The units of $ExtrSi_i$, TAlkSi, TAlkAl, β_i and b were normalized as mg-Si g^{-1}, mg-Si g^{-1}, mg-Al g^{-1}, μmol:μmol and mg-SiO_2 g^{-1} min^{-1}, respectively.

2.2.3. Grain-size Analysis

The grain-size measurement was conducted following an optimum−"PT2SD" protocol proposed by Jaijel et al. (2021). The freeze-dried sediments were added into a 15 mL plastic tube filled with 1 mL Mili-Q water (18 MΩ), then 2 mL of 30% H_2O_2 was mixed with samples for removing the organic matter (addition of the volume of H_2O_2 is dependent on organic matter content of sediment). Then 0.4 mL of Clagon solution was added to the sample solution prior to measurement. Triplicate measurements were applied for grain-size analysis using Malvern Mastersizer 2000 grain-size analyzer with Hydro 2000S module, and an averaged value was calculated after measurements. The mean grain size, specific surface area (SSA), D [3,2] surface area distribution weighted mean (D [3,2]) and fractions of clay (< 2 μm), silt (2 – 62.5 μm) and sand (> 62.5 μm) were also calculated. The definition of textural classification of clay, silt and sand follows the subdivisions introduced by Wentworth (1922). Specific surface area (SSA) of sediment is calculated by the total area of particles divided by the total weight. The D [3,2] is most relevant where specific surface area is important, e.g., reactivity, dissolution and bioavailability, it is sensitive to the presence of fine particulates in the size distribution. Note that the definition of muddy (sand + silt > 70%) and sandy (sand > 50%) sediment follows Flemming (2000).

2.2.4. Chemical Analysis

The chemical analysis includes the measurement of total nitrogen (TN), total organic carbon (TOC) and total carbon (TC). TN, TOC and TC contents were analyzed by flash combustion of precisely weighted sediment samples (about 10 mg) at 950 °C on a

Thermo Scientific FLASH 2000 CHN. Measurement of TOC was conducted using decarbonated (acidification with 1.0 M HCl) sediment. The calculation of inorganic carbon ($CaCO_3$) content is expressed as: $CaCO_3\% = 100*(TC\% - TOC\%)/12$. Detrital material content (detrital% = 100% − TN% − TOC% − $CaCO_3$% − bSi%) was calculated following Rickert (2000). The calibration curve for TN, TOC and TC measurement with $R^2 > 0.9997$ was created by measuring 9 standards which were prepared using N-Phenylacetamide (C_8H_9NO, Sigma-Aldrich 397237), and the analytical precision of TN, TOC and TC was < 5%.

2.2.5. Clay Mineral Analysis

The relative clay mineral (illite, kaolinite, chlorite and montmorillonite) contents were measured by X-ray diffraction (XRD) on oriented mounts of clay-size particles (< 2 μm). All samples were pretreated with 15 mL of 30% H_2O_2 for 24 h to remove the organic matter and then decarbonated using 0.5% HCl. The decarbonated suspensions were washed successively with distilled water to remove excess ions and to enhance the deflocculation of clays. The clay-size particles were separated following Stokes' law and concentrated using a centrifuge. The resulting pastes were spread onto calibrated niches on glass slides. XRD analyses were conducted using a Rigaku D/max 2500 diffractometer with Cu kα radiation (40 KV/150 mA; Speed: 8°/min; Step: 0.024°) at the Qingdao Institute of Marine Geology. Peak areas and illite crystallinity were calculated after manual baseline correction using MacDiff software version 4.2.6 (Petschick, 2002), following the semi-quantitative method of Biscaye (1965).

2.3. Statistical Analysis

To show the distributions of the determined parameters in the studied area, data were plotted using the ODV program, and the values were interpolated in color (Schlitzer, 2023). A Principal Component Analysis (PCA) was performed to identify the majority of the variance among the modeling parameters ($ExtrSi_i$, k_i, TAlkSi, TAlkAl, b, β_j and β_{lin}), sediment physical parameters (clay%, silt%, sand%, mean grain size, D [3,2], sediment-specific surface area, the relative clay mineral contents and water depth,

chemical compositions (bSi%, TN%, TOC%, $CaCO_3$% and detrital%) and the water depth of samples. Two–way Analysis of Variance (ANOVA) were used to test if there are significant differences among the determined parameters. Both PCA and two-way ANOVA tests were performed using Origin 2021b software.

3. Results

3.1. Dissolution of Si and Al Fractions

The analysis of Si and Al data showed that the optimum model for most samples (25/31 samples) is model 2, and 6 samples (A4, B09, C4, NSCS1, NSCS7 and NSCS10) were only fitted with model 1. The determined parameters showed a heterogeneous distribution of alkaline extracted Si and Al in surface sediments of the Chinese marginal Seas. Figure 2 shows the distribution of non-linear dissolving Si phases ($ExtrSi_1$: 0.21 – 5.97 mg-Si g^{-1}, $ExtrSi_2$: 0.16 – 6.01 mg-Si g^{-1}), total alkaline extracted Si (TAlkSi: 0.65 – 23.31 mg-Si g^{-1}) and Al (TAlkAl: 0.14 – 5.79 mg-Si g^{-1}) as well as the dissolution rate of silicate minerals (b: 0.02 – 0.36 mg-SiO_2 g^{-1} min^{-1}). The distribution patterns of $ExtrSi_1$, $ExtrSi_2$, TAlkSi, TAlkAl and b values were similar with high values in sediments of the western BH, northern YS, Zhe-Min coast and the ECS continental slope. In addition, as shown in Figure A1, the reactivity and the Si:Al ratio of the first non-linear dissolving Si fraction (k_1: 0.06 – 4.50 min^{-1}; β_1: 2.00 – 36.07) were higher than the second non-linear dissolving Si fraction (k_2: 0.05 – 0.13 min^{-1}; β_2: 1.83 – 7.84), and the Si:Al ratio of non-linear dissolving Si fractions (β_1 and β_2) were larger than the Si:Al ratio of the linearly dissolving silicate mineral (β_{lin}: 1.57 – 5.07).

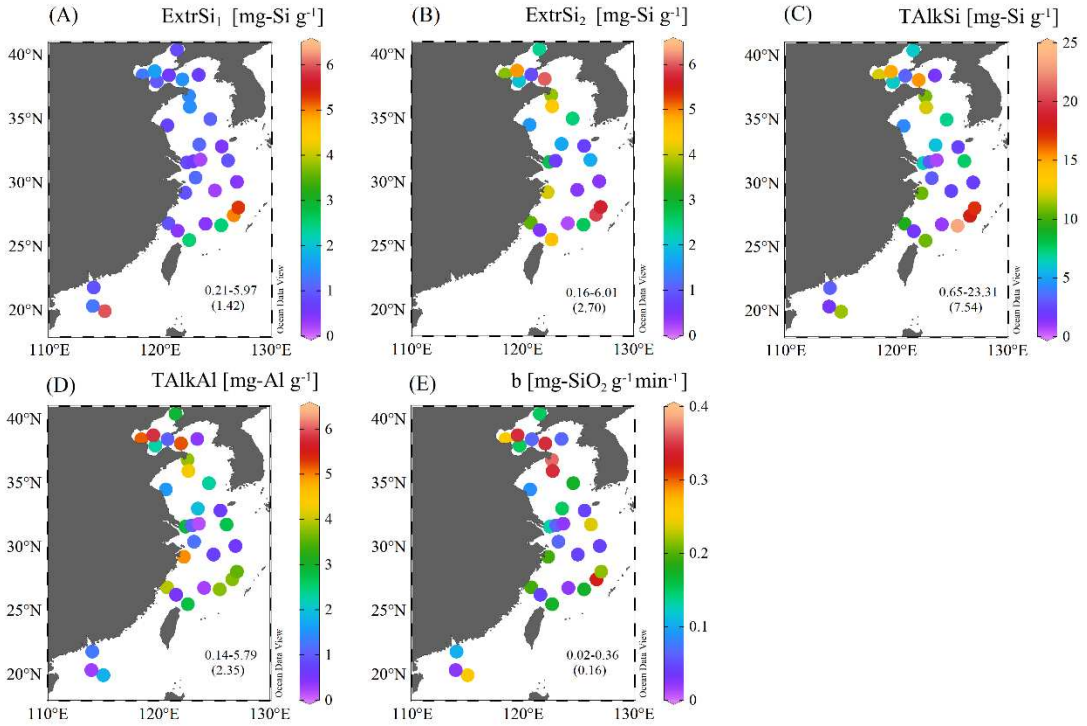

Figure 2. The parameters (A: *ExtrSi*$_1$, first non-linearly dissolving Si phase; B: *ExtrSi*$_2$, second non-linearly dissolving Si phase; C: TAlkSi: the total amount of Si; D: TAlkAl, the total amount of Al; and E: *b*, dissolution rate of the linearly dissolving silicate mineral) of the simultaneous alkaline extraction, which was interpolated in color. The values in each plot represent the ranges and averages (shown in brackets) of data, all the determined parameters were presented in Table S1. The figure was generated using the ODV program (Schlitzer, 2023).

3.2. Grain-size Distributions

Grain size is a key physical parameter of marine sediments. Generally, the sediments used in this study contain mainly silt (54.1%), sand (41.9%) and with minor amount of clay (3.9%) content. The mean grain-size distribution at the study area is similar to the sand distribution whereas the distribution of specific surface area of the sediments is similar to the distribution of clay and silt fractions (Figure 3). Further, areas characterized by fine grain-size fractions (clay and silt: grain-size < 62.5 μm) were found in the western BH, northern YS, Zhe-Min coast and ECS continental slope (Figure 3 A and B). The outer continental shelf of ECS is characterized by high sand content (Figure 3 C). The largest mean grain size was found in a sample (NSCS10,

Figure 3 D) from the NSCS. Our determined values are in agreement with the previously reported grain-size distribution patterns (Wu and Wen, 2019; Shi et al., 2021; Mei et al., 2020; Ma et al., 2023).

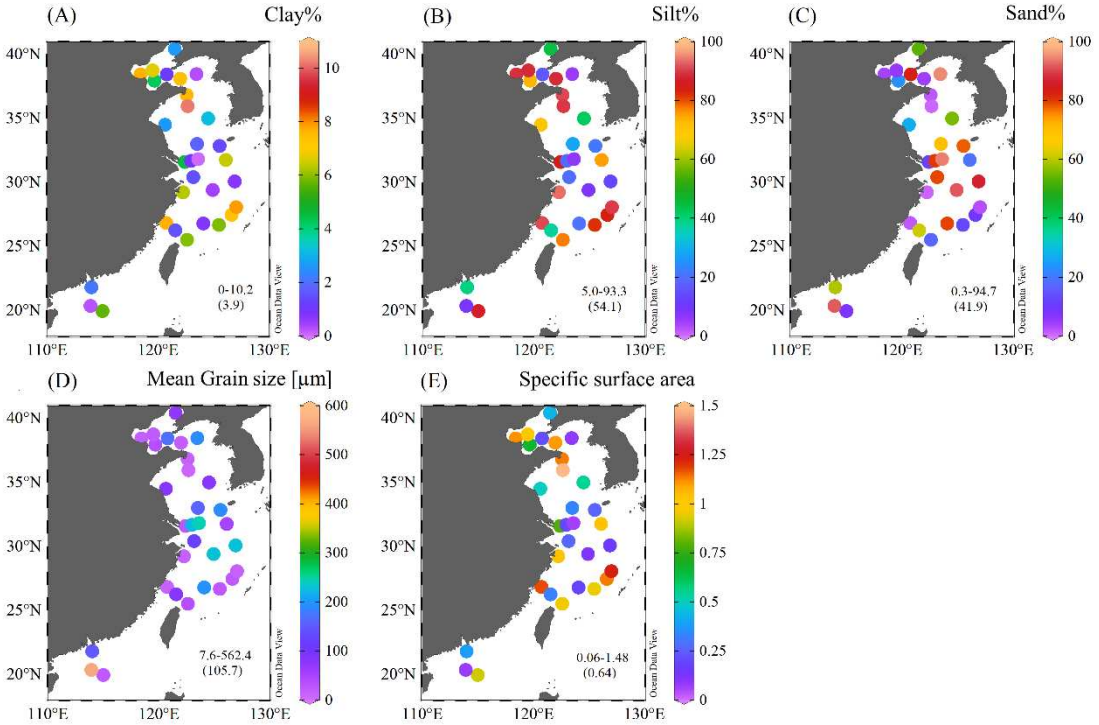

Figure 3. The clay% (A), silt% (B), sand% (C), mean grain size (D) and specific surface area (E) of surface sediments. The values in each plot represent the ranges and averages (shown in brackets) of data, all the determined parameters were presented in Table S1. The figure was generated using the ODV program (Schlitzer, 2023).

3.3. Chemical Parameters

The distribution of detrital material, bSi, $CaCO_3$, TN and TOC contents are shown in Figure 4. Samples from the study area contain high detrital material (average: 90.8%, Figure 4 A), which agrees with previous studies (Wu and Liu, 2020; Ma et al., 2023). A higher content of detrital material was found in near-shore sediments than in sediments on the ECS continental shelf. The distribution of bSi% and $CaCO_3$% (Figure 4 B, C) showed similar patterns with higher values in near-shore sediments and deep-water sediments (i.e., continental slope). Distributions of TN% and TOC% were similar (Figure 4 D, E) with high values in the central YS and the continental slope of ECS.

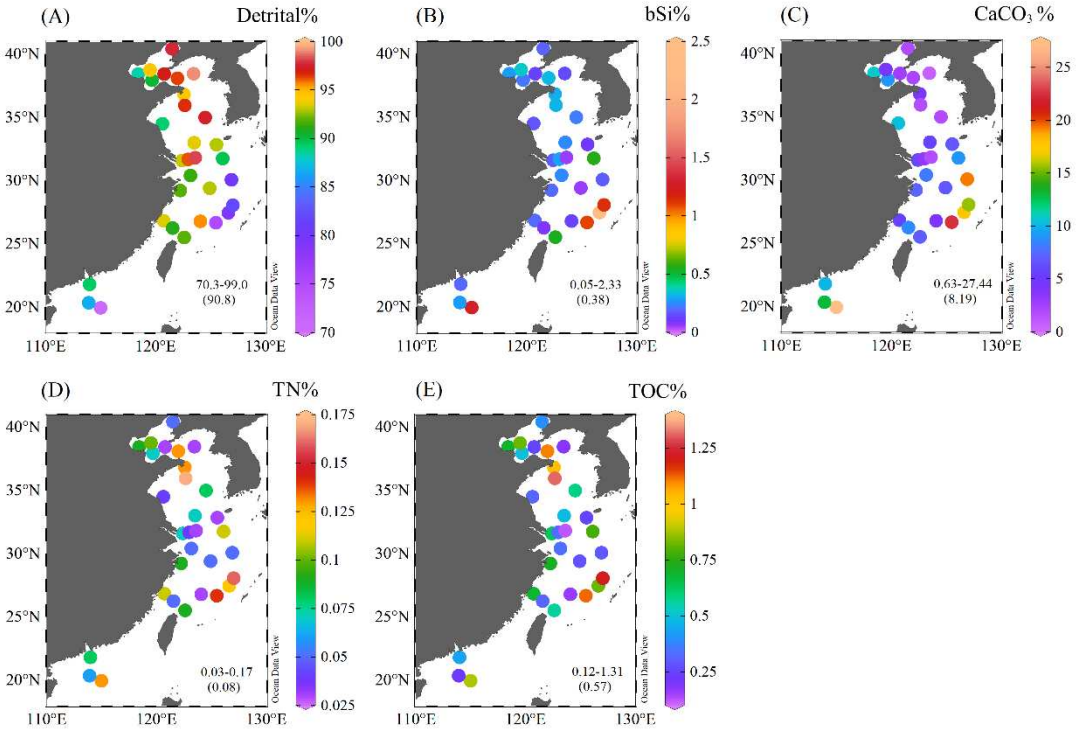

Figure 4. Detrital material content (A), bSi% (B), $CaCO_3$% (C), TN% (D) and TOC% (E) of the study area. The values in each plot represent the ranges and averages (shown in brackets) of data, all the determined parameters were presented in Table S1. The figure was generated using the ODV program (Schlitzer, 2023).

3.4. Clay Minerals

The relative clay mineral compositions of the study area were illite (63.5%), chlorite (20.4%), kaolinite (11.9%) and montmorillonite (4.3%). Generally, illite and chlorite content increase from the BH to ECS (Figure 5 A, B), whereas a reverse pattern was found for kaolinite (Figure 5 C). The BH sediments contain higher montmorillonite content than other regions (YS, ECS and SCS) of this study (Figure 5 D). In addition, samples from BH and western YS and the inner shelf of ECS have higher illite crystallinity (> 0.28) than the other samples (Figure 5 E). This indicates a poor illite crystallinity of near-shore sediments.

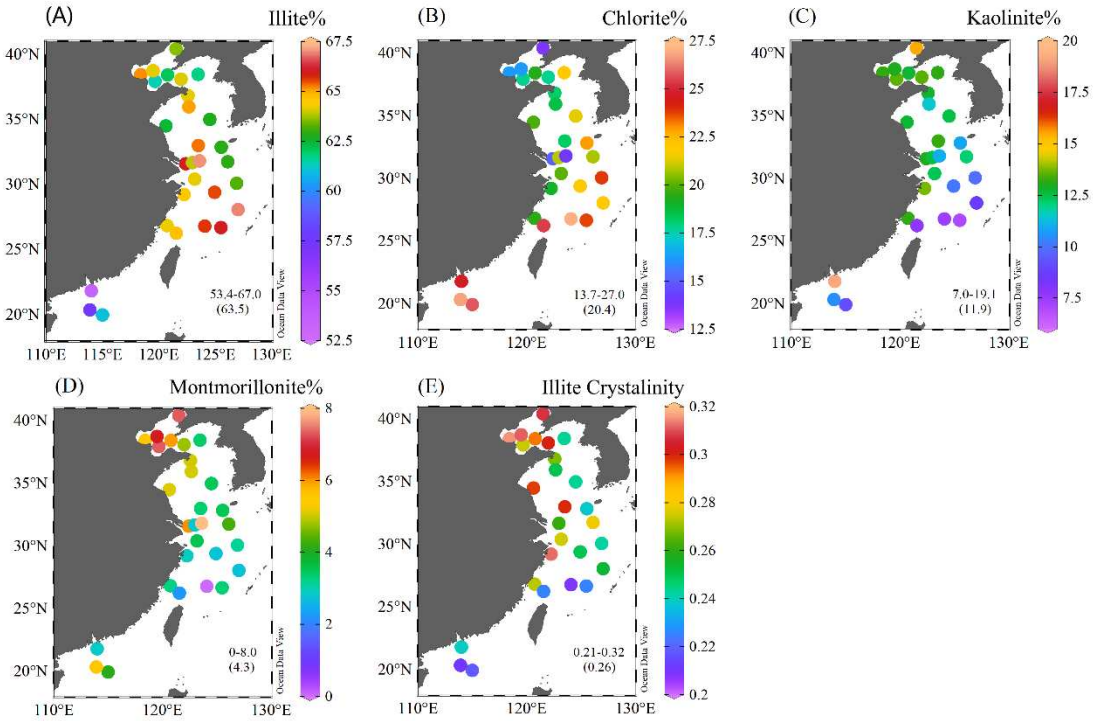

Figure 5. The illite% (A), chlorite% (B), kaolinite% (C), montmorillonite% (D) and illite crystallinity (D) of the sediments. The values in each plot represent the range of data and the average value, all the determined parameters were presented in Table S1. The figure was generated using the ODV program (Schlitzer, 2023).

3.5. Principal Component Analysis

The PCA displayed relationships between alkaline extraction parameters and sediment physical and chemical properties. The distributions of muddy and sandy seidments on the bi-plot were also presented (Figure 6). Results showed positive relationship of the continuous alkaline extraction results ($ExtrSi_1$, $ExtrSi_2$, b, β_1, β_2, β_{lin}, bSi%, TAlkSi and TAlkAl), TOC%, TN%, clay%, silt%, SSA, the parameters of clay minerals (illite crystallinity, illite%, montmorillonite%) and sediment water depth. The β_1, k_1 and k_2 were positively related to mean size of sediment, sand%, detrital%, D [3,2] and chorite%, kaolinite%, and were negatively related to fine-size fractions (clay% and silt%), SSA, b, TAlkSi, TAlkAl, TOC%, TN%, $ExtrSi_i$, bSi% $CaCO_3$%, β_{lin} and parameters of clay minerals.

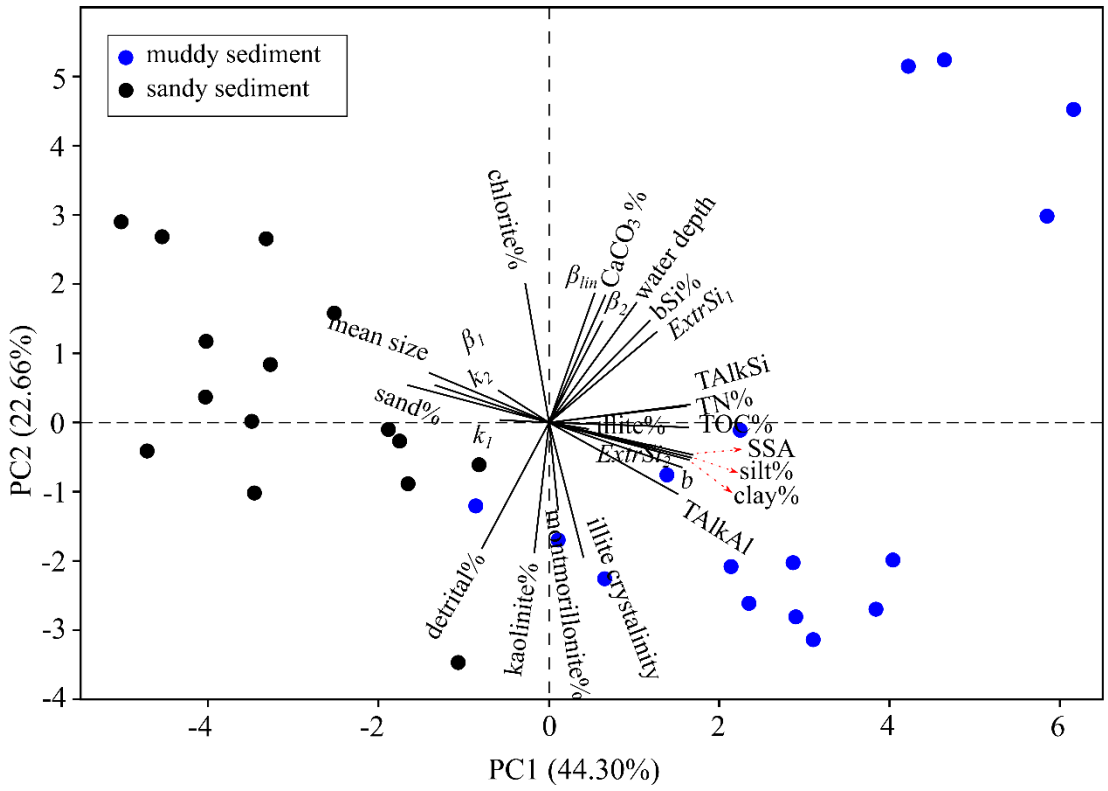

Figure 6. Bi-plot of PCA ordination of the determined parameters for all samples. PC1 represents principle component 1 and PC2 represents principle component 2. The symbols in blue and black color represent muddy and sandy sediments, respectively.

4. Discussion

4.1. Muddy Sediments Release more Si and Al than Sandy Sediments

Sediment samples of this study were grouped as sandy sediment (sand > 50%, SSA < 0.5) and muddy sediment (clay + silt > 70%, SSA > 0.5). The results showed that values for the alkaline extracted Si and Al from muddy sediments were much higher (> 200%) than those for the sandy sediments, which indicates that muddy sediments could be an important source of Si and Al in the Chinese marginal Seas. As shown in Figure 7, values for the alkaline extracted TAlkSi, TAlkAl, bSi and silicate mineral contents from muddy sediments were 2 to 3 times higher than values determined for sandy sediments. In addition, the alkaline leachable silicate minerals contents outweigh bSi% from both muddy and sandy sediments (Figure 7). Therefore, although the reactivity of bSi is higher than silicate minerals (see Figure A1 and section 3.1), the dissolution of

silicate minerals is potentially an important Si source for the Chinese marginal Seas because bSi% (bSi% < 2%) is much lower than the detrital% (average: 90.8%, Figure 4) and the physical mass of silicate minerals (> 70%, Wu and Liu, 2020). Thus, the dissolution of silicate minerals is an important potential source of Si in coastal shelf systems (i.e., CCMZs) (Jeandel and Oelkers, 2015; Pickering et al., 2020). A comparison of alkaline leachable Si and Al from different sediment types further confirmed the important role of muddy sediments on Si release. Samples containing more fine-size fractions (< 62.5 μm) released more Si (TAlkSi, bSi and silicate minerals) and TAlkAl (ANOVA test: $p < 0.001$, Figure 8). This positive relationship is probably due to three reasons: 1) high specific surface area (SSA) of sediment, 2) species of diatoms in sediments and their cell sizes and 3) better conservation of bSi in muddy sediments. Detailed explanations are presented in the following separate paragraphs.

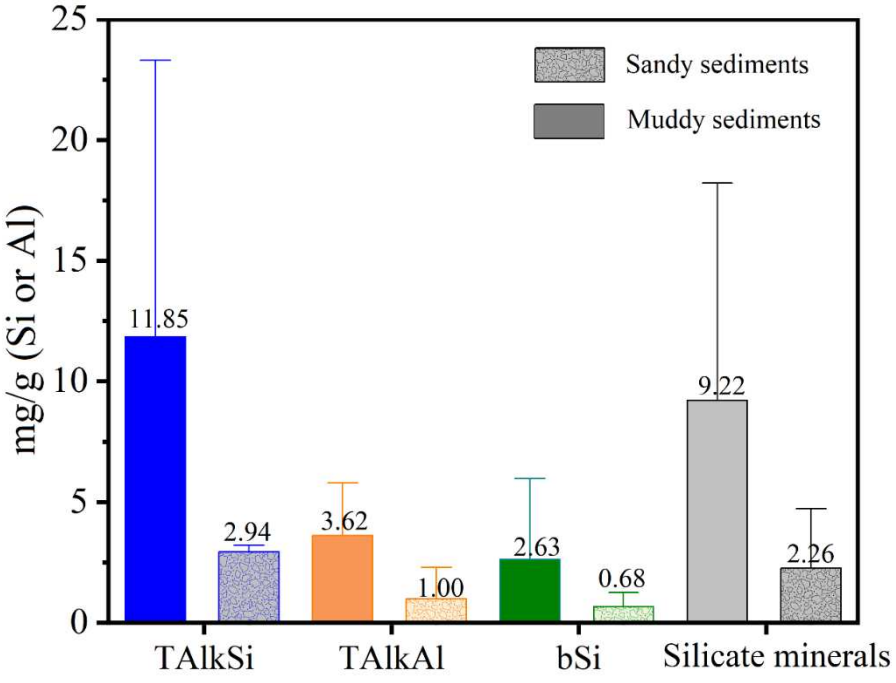

Figure 7. Plot of alkaline extracted Si (TAlkSi, bSi, silicate minerals) and Al (TAlkAl) from muddy and sandy sediments. Error bars represent the data range with 1.5 IQR (Interquartile Range), and the numbers above the bar chart represent mean values. The averaged values and errors were calculated using data of all sampling sites of this study.

Dissolution of silica (bSi and silicate minerals) in solution is controlled by

temperature, pH and surface area of solid particles (Niibori et al., 2000; Dixit and Van Cappellen, 2002; Van Cappellen et al., 2002; Cama and Ganor, 2015). Therefore, under temperature and pH-controlled experimental conditions, the dissolution kinetics of Si and elements combined with Si (i.e., Al (Gehlen et al., 2002; Koning et al., 2002; Loucaides et al., 2010), Fe (Liao et al., 2023) and Ge (Mortlock and Froelich, 1989; Sutton et al., 2018; Baronas et al., 2019)) are dependent on the SSA of the particles. As shown in Figure 6 and Figure A2, SSA has a positive relationship with the clay% and silt%, and is negatively related to sand% and the D [3,2] surface weighted mean. Therefore, an increased yield of alkaline extracted Si and Al phases from muddy sediments (see Figure 7) is linked to larger SSA.

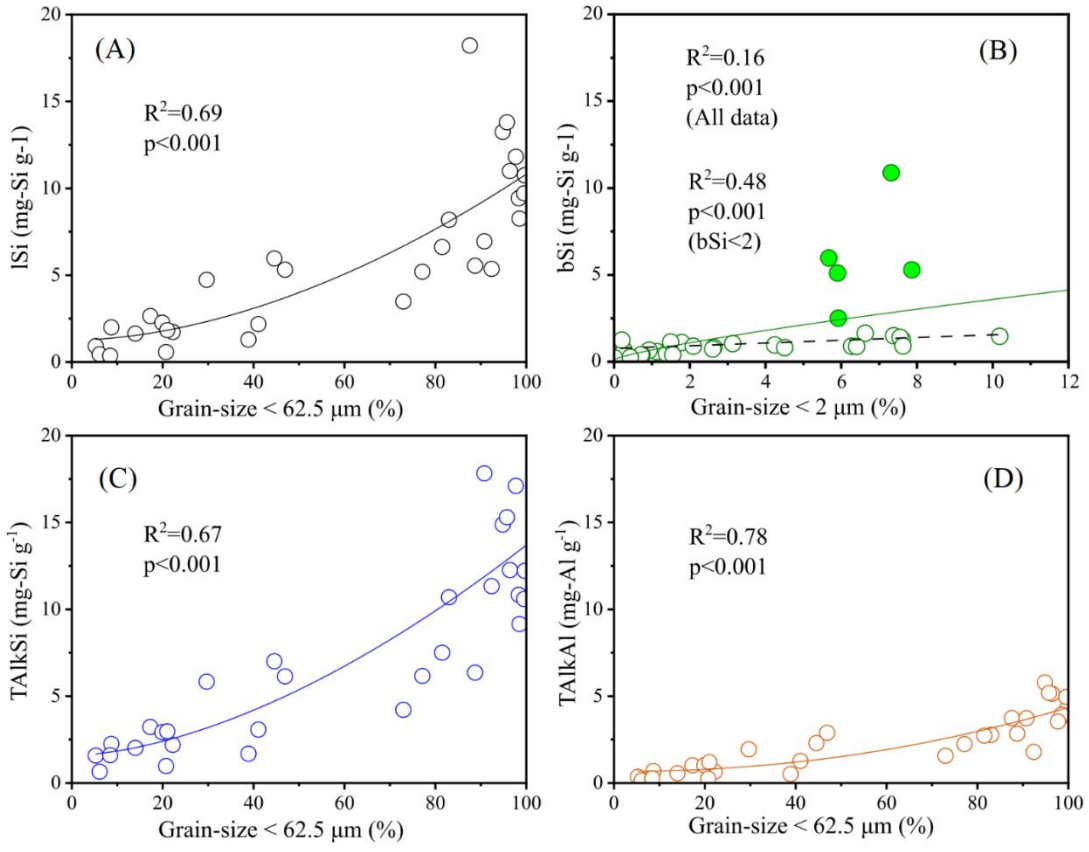

Figure 8. Relation of alkaline extracted Si and Al and sediment grain-size content. Samples containing a higher percentage of fine grains potentially release more (A) silicate minerals, (B) bSi, (C) TAlkSi and (D) TAlkAl. The dots filled in green color (see plot B) represent samples from the continental slope of ECS (C12, D12, DC and F8) and SCS (NSCS7).

Another reason that could cause an enhanced Si and Al dissolution from muddy sediments is attributed to bSi types and sizes given their different solubilities (Maldonado et al., 2022). Several types of bSi (diatom, radiolarian, sponge spicules and phytolith) were found in sediments of the Chinese marginal Sea (Chen et al., 2014; Zhang et al., 2015; Ran et al., 2018; Qu et al., 2020; Zhu et al., 2023). However, phytoliths were mainly found in sediments of river estuaries (Ran et al., 2018). Radiolarian tests and sponge spicules were more abundant in sediments of the continental slope of the ECS and SCS basin (Chou et al., 2012; Zhang et al., 2015; Zhu et al., 2023). Whereas diatoms were the major types of bSi in sediments of the continental shelf of the Chinese marginal Seas. Based on the measurement of bSi% in various sediment size fractions and the scanning electron microscopic observations, Wang et al. (2014) found the largest bSi% in the sediment size fraction of < 16 μm, and the microscopic measurements showed most of the diatoms were nano-diatoms with a diameter smaller than 14 μm (dominant cells diameters: 2 – 14 μm). Thus, the presence of nano-diatoms in sediment may be one of the reasons that cause the positive relationship observed between bSi% vs. muddy sediment. In addition, the presence of sponge spicules and radiolarians may affect our interpretations. There are five samples (filled symbols) characterized by higher bSi% than other sediments (bSi: TOC% as shown in Figure A3 B; the slope of TAlkSi vs. TAlkAl plot as shown in Figure A4), indicating better bSi preservation. These samples were located at the continental slope of the ECS and NSCS deep water (> 500 m) and contains sponge spicules and radiolarians (Zhang et al., 2015; Zhu et al., 2023) that are more resistant to dissolution than diatoms (Hurd, 1983). Thus, sediments of CCMZs containing more sponge spicules and radiolarians are characterized by higher bSi%: TOC% ratios.

Further, a better preservation of bSi in muddy sediments also induces elevated values for leachable Si and Al. The positive correlation of the $ExtrSi_1$ (represents bSi), $ExtrSi_2$ (represents silicate minerals for most samples except sample DC and D12, see Table S1), TOC%, TAlkAl and SSA (Figure 6) indicated a good preservation of TOC%, $ExtrSi_1$ and $ExtrSi_2$ in muddy sediments as compared to sandy sediments. Krause et al. (2017) and Pickering et al. (2023) found a strong correlation between TOC% and the

authigenic alternation of bSi in sediments of Mississippi River delta, and concluded that the increasing of organic content may impact the diagenetic modification of bSi. Thus, one possible mechanism for the enhanced preservation of bSi is attributed to the favorable formation of authigenic silicate in high TOC% muddy sediments that generated $ExtrSi_2$ and enhanced the preservation of $ExtrSi_1$. Our previous study defined $ExtrSi_2$ as lithogenic silica (authigenic silicates and/or clay minerals) (Zhu et al., 2023). Through comparing the modeling parameters and the sediment physical and chemical parameters, $ExtrSi_2$ is likely an authigenic alumino-silicate phase. However, further studies applying multiple geochemical tools (δ^{30}Si, Si, Al, Fe, K; Pickering et al., 2020; Huang et al., 2023; ^{32}Si and Si, Rahman et al., 2016) are needed in order to define the $ExtrSi_2$ phase specifically.

4.2. Al from Silicate Minerals Hindering the Dissolution of bSi in Sediments

Our results confirm that the dissolution (reactivity) of bSi in sediments is hindered by the structural incorporation of Al that originates from silicate minerals. It suggests that this decreased reactivity of bSi leads to enhanced opal preservation in muddy sediments of CCMZs.

We found the reactivity (k_1) and Si:Al ratio of bSi (β_1) decrease with the increase of sedimentary SSA (Figure 6 and Figure 9). The decrease in bSi reactivity in muddy sediments (Figure 9 A, B) is explained by an increased amount of Al incorporated with bSi surface, because the Al uptake by bSi surfaces takes place in the sediments during early diagenesis can generate alumino-silicate “coating” that prevents further dissolution of biogenic silica (Van Cappellen and Qiu, 1997; Dixit et al., 2001). In addition, the previous study used Scanning Electron Microscopy coupled with an Energy Dispersive Spectrometer (SEM-EDS) to qualitatively measure element distributions at the diatom surface and found enriched Al in sedimentary diatom frustules of ECS (Zhu et al., 2023), which further confirms our findings. The decreased bSi reactivity also explains why bSi% is higher in muddy sediments than in sandy sediments.

Further, we argue that the Al incorporated with bSi structures mostly originates from

the dissolution of silicate minerals. Siliceous frustules produced in the photic zone contain a trace amount of Al (Si:Al > 120 (van Bennekom et al., 1989; Rickert et al., 2002; Koning et al., 2007)). During the deposition and burial of bSi, a diagenesis process (such as reverse weathering process (Michalopoulos and Aller, 2004; Ehlert et al., 2012)) with diagenetic Al uptake (Ren et al., 2013; Dixit et al., 2001) starts increasing the Al content of bio-siliceous structures in the sediments (Si:Al < 50) (van Bennekom et al., 1989; Van Beusekom et al., 1997; Rickert et al., 2002; Ren et al., 2013). Our results showed high Al (Si:Al < 40, Figure 9 B) contents in bSi of Chinese marginal Seas' sediments, with especially high Al contents (Si:Al < 10) in bSi observed in sediments characterized by high SSA (i.e., the muddy sediments that contain silicate minerals with high dissolution rate, see Figure 9 D). This is likely due to the incorporation of Al with bSi on the seafloor, because the dAl concentration of pore water and the overlying water at the sediment-water interface (> 120 nM (Mackin and Aller, 1984)) are much higher than the dAl concentration of the water column (< 50 nM (Ren et al., 2006; Li et al., 2018; Zhang et al., 2020)), and the residence time of bSi at the seafloor overtake the time of settling from the surface to bottom water (15 – 70 m d^{-1} (Passow, 1991; Ran et al., 2015)). It is, therefore, reasonable to attribute the major source of Al that is incorporated with bSi to Al release during silicate mineral dissolution (Dixit et al., 2001).

The Al released from silicate minerals hinders the dissolution of bSi in sediment and impacts the accurate determination of bSi%. Studies have found incomplete digestion of bSi due to alumino-silicate coatings on bio-siliceous structures (Zhu et al., 2023), resulting in an underestimation of the bSi%. Moreover, changes in the sediment depositional environment can affect the release of Al from silicate minerals (Mackin and Aller, 1984; Measures and Hatta, 2021; Pickering et al., 2023), which subsequently influence the incorporation of Al and bSi structures and the preservation of bSi in sediments. Therefore, attention should be paid to both the Si:Al ratio and the types of bSi when using bSi% to understand past environmental changes.

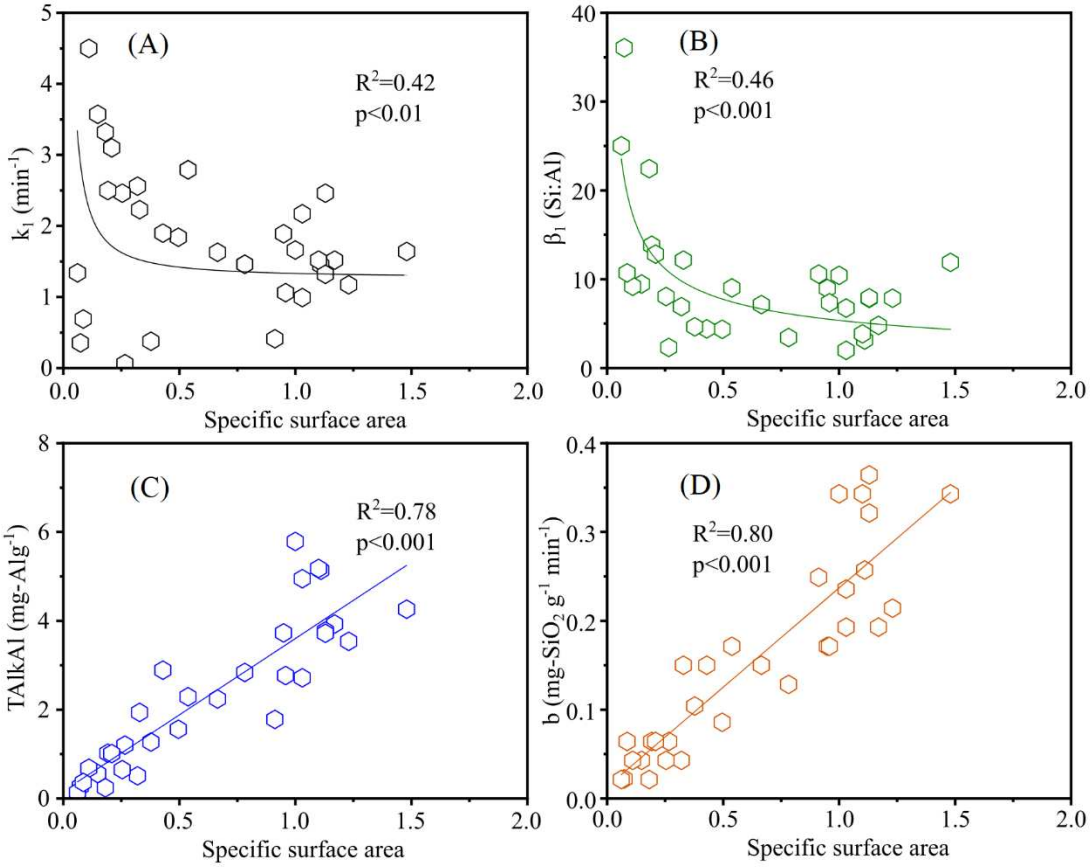

Figure 9. Relationship of grain-size specific surface area (SSA) and bSi reactivity constant (A), Si:Al ratio (β_1) of bSi (B), TAlkAl (C), and silicate mineral dissolution rate (b) (D).

4.3. Implications of Simultaneous Alkaline Extraction of Si and Al

The simultaneous alkaline extraction of Si and Al is widely applied for differentiating various Si phases (Koning et al., 2002; Barão et al., 2015; Raimonet et al., 2015; Zhu et al., 2023). The definition of the alkaline extracted Si from silicate minerals is based on an assumption of a slow linear dissolution of clay minerals (Koning et al., 2002). The distinct different Si:Al ratios between bSi (Si:Al > 5) and clay (Si:Al < 5) allow an accurate measurement of bSi-poor sediments that contain high silicate minerals, e.g., CCMZs of Chinese marginal Seas and the Amazon shelf (Koning et al., 2002).

Previous studies found the Si:Al ratios and the reactivity of bSi are dependent on bSi types, 'aging' (Hurd, 1983; Van Cappellen and Qiu, 1997; Dixit et al., 2001; Van Cappellen et al., 2002) or diagenetic alteration of bSi (Huang et al., 2023). Therefore, the reactivity and Si:Al ratio of bSi calculated by non-linear dissolution models cannot

be used to compare samples of different depositional environments (Koning et al., 2002). However, the dissolution rate of silicate minerals (b) in hot alkaline solutions is dependent on the SSA of solid particles, and the β_{lin} is dependent on the clay mineral compositions (type and content) of sediments. By comparing with previously published data (Figure 10), we found β_{lin} reflects the major types of clay minerals of sediments. For example, the β_{lin} of the kaolinite-rich Congo deep-sea fan sediments (1.16 − 1.18, Barão et al., 2015) are equal to the Si:Al ratio of kaolinite (1.10 – 1.18, Kamatani and Oku, 2000; and Koning et al. 2002). The β_{lin} of the kaolinite and montmorillonite-rich Angola basin (1.90 – 2.15, Koning et al., 2002) sediments are within the Si:Al ratios of kaolinite and montmorillonite (1.10 – 4.80, Kamatani and Oku, 2000, and Koning et al., 2002). The β_{lin} of the illite-rich Iberian margin sediments (2.23 – 2.34, Koning et al., 2002) are similar to illite (2 – 2.47, Kamatani and Oku, 2000 and Koning et al., 2002). In addition, the clay minerals in the sediment of Tokyo Bay are mainly illite (50%) and montmorillonite (40%), and reflected in an alkaline extracted Si:Al ratio of 2.41 (Kamatani and Oku, 2000). Further, positive relationship between β_{lin} and major type of clay was also shown in Figure 6. The β_{lin} of sediments from Chinese marginal Seas (β_{lin} = 2 – 3) are within the range of Si:Al ratio of illite with exceptions for SCS samples, which have higher kaolinite or illite content (Figure 10). Therefore, β_{lin} values represent the Si:Al ratios of major types of clay minerals in CCMZs sediments. The correlation between the calculated β_{lin} values and Si:Al ratios of major types of clays is due to the high solubility of clay minerals as compared with other crystalized silicates (such as quartz and feldspar) and the quantity of the clay-size fractions in sediments (~10% of total sample volume). Further, whether this correlation can be applied to other sediment types is not clear. The β_{lin} of opal-rich samples (Equatorial Pacific: β_{lin} > 9 (Barão et al., 2015), particulate bSi sample: β_{lin} = 48 (Koning et al.,

2002)) and beach sand sample (Texel, North Sea: β_{lin} = 6.9 (Koning et al., 2002)) are characterized by high Si:Al ratios (> 5), which is higher than the Si:Al ratio of clay minerals (Si:Al < 5). Further studies should check whether these values are an artifact caused by inappropriate modeling or due to the sediment mineral compositions.

Considering that simultaneous analysis of the Si and Al provides information on the digestion of both bSi and silicate minerals, it can be adapted to the flow-through experiment for quantifying the dissolution of bSi and non-bSi at the sediment-water interface under in-situ conditions. The calculated β_i represents Si:Al ratio of bSi and it decreases during the bSi deposition and burial process (order of β_i: fresh diatom > diatom in surface sediment > diatom in deep sediment) (Koning et al., 2002). Thus, the β_i value can reflect the level of diagenetic alteration of bSi in the sediment of the same marine regions (Koning et al., 2002).

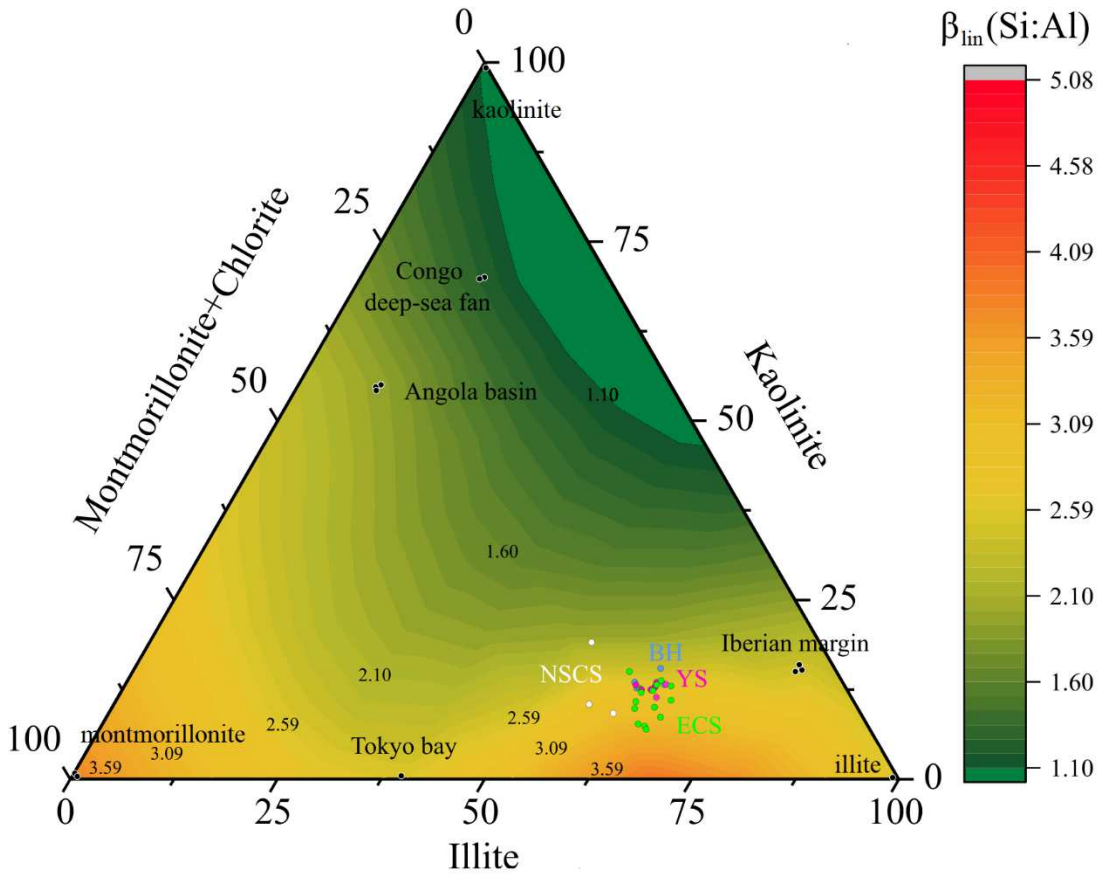

Figure 10. Relative clay mineral (illite, kaolinite and montmorillonite+chlorite) content

of sediment and the Si:Al ratio of silicate minerals (β_{lin}) calculated from the continuous alkaline extraction of Si and Al. The color bar represents the β_{lin} values. Numbers within the plot are contours calculated based on determined β_{lin}. Data sources of clay mineral composition: 1) Congo deep-sea fan, Angola basin and Iberian margin: Griffin et al. (1968); 2) Tokyo Bay: Oinuma and Kobayashi (1966); 2) Clay minerals (illite, kaolinite and montmorillonite): Kamatani and Oku (2000) and Koning et al. (2002). 4) Chinese marginal Seas (BH, YS, ECS, SCS): this study. Data sources of Si:Al ratio of silicate minerals (β_{lin}) from simultaneous alkaline extraction of Si and Al: 1) Congo deep-sea fan: Barão et al. (2015); 2) Angola basin and Iberian margin: Koning et al. (2002); 3) Tokyo Bay: Kamatani and Oku (2000); 4) BH, YS and ECS: Zhu et al. (2023); 5) SCS: this study. All sediment samples were selected from regions under strong influence of terrestrial input and with high silicate minerals content.

5. Conclusion

We conducted simultaneous alkaline extraction of Si and Al in sediments of Chinese marginal Seas and measured the physical and chemical properties of sediments to understand the incongruent dissolution of silicate minerals in sediments of CCMZs. Our results demonstrated that more Si (sourced from bSi and silicate minerals) and Al dissolve from muddy sediments than from sandy sediments. Although the dissolution rate of silicate minerals is slower than that of bSi, their contribution to the reactive Si pool is greater due to their larger quantities as compared to bSi. This suggests that muddy sediments are an important potential Si source for the CCMZs of Chinese marginal Seas. We found that decreased bSi reactivity is correlated with low Si:Al ratios, especially for samples of muddy deposits. The source of Al is likely originating from silicate minerals dissolution. The incorporation of Al into bio-siliceous structures hinders the dissolution of bSi, thus enhancing bSi preservation. The preservation efficiency may vary among different types of bSi. Applying continuous alkaline extraction methods can help to understand these differences due to its ability to differentiate Si phases with different dissolution rates. Further, the modeling parameters of the simultaneously analyzed Si and Al concentrations uncover the major types of clay minerals existing in CCMZs sediments because of their different chemical characteristics (Si:Al ratios), but whether they can be applied to sediments of open ocean and/or sandy beaches require dedicated studies.

Acknowledgements

This study represents partial fulfillment of the requirements for the Ph.D. thesis of DZ at the Ph.D. course of the Ocean University of China and the Université de Bretagne Occidentale. DZ would like to thank Prof. Zuosheng Yang and Dr. Stefan Lalond for the helpful discussions. DZ also thank all members at SML's group, the CHIBIDO LAB (LEMAR: Laboratory of Environmental Marine Sciences) and the Department of Biology (University of Antwerp) for their help and assistance during this study. Special thanks to Dr. Laura M. Wehrmann and two anonymous reviewers for their insightful comments on our manuscript.

Funding

This study was funded by the Natural Sciences Foundation of China (NSFC: 42176040, U1806211), the Taishan Scholars Program of Shandong Province, Aoshan Talents Program Supported by the Qingdao National Laboratory for Marine Science and Technology (No. 2015ASTP-OS08), and was supported by the French National Research Agency (18-CEO1-0011-01) and the ISblue project, Interdisciplinary graduate school for the blue planet (ANR-17-EURE-0015) and co-funded by a grant from the French government under the program "Investissements d'Avenir" embedded in France 2030.

Author contributions

DZ, SML, JNS, AL, PT designed this study and wrote the original draft. DZ conducted the experiments, did the data analysis. DZ, SML, JNS, AL, PT, JR, JS and YM wrote, reviewed and edited the manuscript.

Declaration of Competing Interest

The authors declare that they have no known competing financial interests or personal relationships that could have appeared to influence the work reported in this paper.

Data availability

Data will be made available on request.

References:

Amann, T., Hartmann, J., Struyf, E., De Oliveira Garcia, W., Fischer, E. K., Janssens, I., Meire, P., Schoelynck, J., 2020. Enhanced weathering and related element fluxes - a cropland mesocosm approach. *Biogeosciences* 17, 103–119. doi: 10.5194/bg-17-103-2020.

Armstrong, R. A., Lee, C., Hedges, J. I., Honjo, S., Wakeham, S. G., 2002. A new, mechanistic model for organic carbon fluxes in the ocean based on the quantitative association of POC with ballast minerals. *Deep. Res. Part II Top. Stud. Oceanogr.* 49, 219–236. doi: 10.1016/S0967-0645(01)00101-1.

Barão, L., Clymans, W., Vandevenne, F., Meire, P., Conley, D. J., Struyf, E., 2014. Pedogenic and biogenic alkaline-extracted silicon distributions along a temperate land-use gradient. *Eur. J. Soil Sci.* 65, 693–705. doi: 10.1111/ejss.12161.

Barão, L., Vandevenne, F., Clymans, W., Frings, P., Ragueneau, O., Meire, P., Conley, D. J., Struyf, E., 2015. Alkaline-extractable silicon from land to ocean: A challenge for biogenic silicon determination. *Limnol. Oceanogr. Methods* 13, 329–344. doi: 10.1002/lom3.10028.

Baronas, J. J., Hammond, D. E., Rouxel, O. J., Monteverde, D. R., 2019. A first look at dissolved ge isotopes in marine sediments. *Front. Earth Sci.* 7. doi: 10.3389/feart.2019.00162.

Biscaye, P. E., 1965. Geological Society of America Bulletin Mineralogy and Sedimentation of Recent Deep-Sea Clay in the Atlantic Ocean and Adjacent Seas and Oceans. *Geol. Soc. Am. Bulletim* 76, 803–832. doi: 10.1130/0016-7606(1965)76.

Cama, J., Ganor, J., 2015. Dissolution Kinetics of Clay Minerals, in T. Christophe, I. S. Carl, C. B. Ian, and B. Faqpza (Eds.), Developments in Clay Science, Elsevier Ltd., Amsterdam, pp. 101–153. doi: 10.1016/B978-0-08-100027-4.00004-8.

Chen, C., Zhao, G., Chen, M., Lan, D., Lan, B., 2014. Diatom distribution in surface sediments from Chinese inshore waters and the relationship to modern environmental variables. *Chinese J. Oceanol. Limnol.* 32, 828–844. doi: 10.1007/s00343-014-3194-3.

Chou, Y., Lou, J. Y., Chen, C. T. A., Liu, L. L., 2012. Spatial distribution of sponge spicules in sediments around Taiwan and the Sunda Shelf. *J. Oceanogr.* 68, 905–912. doi: 10.1007/s10872-012-0143-7.

Dixit, S., Van Cappellen, P., 2002. Surface chemistry and reactivity of biogenic silica. *Geochim. Cosmochim. Acta* 66, 2559–2568. doi: 10.1016/S0016-7037(02)00854-2.

Dixit, S., Van Cappellen, P., Van Bennekom, A. J., 2001. Processes controlling solubility of biogenic silica and pore water build-up of silicic acid in marine sediments. *Mar. Chem.* 73, 333–352. doi: 10.1016/S0304-4203(00)00118-3.

Ehlert, C., Grasse, P., Mollier-Vogel, E., Böschen, T., Franz, J., F.de Souza, G., Reynolds, B. C. Stramma, L., Frank, M., 2012. Factors controlling the silicon isotope distribution in waters and surface sediments of the Peruvian coastal upwelling. *Geochim. Cosmochim. Acta* 99, 128–145. doi:

10.1016/j.gca.2012.09.038.
Fabre, S., Jeandel, C., Zambardi, T., Roustan, M., and Almar, R., 2019. An Overlooked Silica Source of the Modern Oceans: Are Sandy Beaches the Key? *Front. Earth Sci.* 7, 1–13. doi: 10.3389/feart.2019.00231.
Flemming, B. W., 2000. A revised textural classification of gravel-free muddy sediments on the basis of ternary diagrams. *Cont. Shelf Res.* 20, 1125–1137. doi: 10.1016/S0278-4343(00)00015-7.
Frings, P., 2017. Revisiting the dissolution of biogenic Si in marine sediments: a key term in the ocean Si budget. *Acta Geochim.* 36, 429–432. doi: 10.1007/s11631-017-0183-1.
Gallinari, M., Ragueneau, O., Corrin, L., DeMaster, D. J., Tréguer, P., 2002. The importance of water column processes on the dissolution properties of biogenic silica in deep-sea sediments I. Solubility. *Geochim. Cosmochim. Acta* 66, 2701–2717. doi: 10.1016/S0016-7037(02)00874-8.
Gallinari, M., Ragueneau, O., DeMaster, D. J., Hartnett, H., Rickert, D., Thomas, C., 2008. Influence of seasonal phytodetritus deposition on biogenic silica dissolution in marine sediments-Potential effects on preservation. *Deep. Res. Part II Top. Stud. Oceanogr.* 55, 2451–2464. doi: 10.1016/j.dsr2.2008.06.005.
Gehlen, M., Beck, L., Calas, G., Flank, A. M., Van Bennekom, A. J., Van Beusekom, J. E. E., 2002. Unraveling the atomic structure of biogenic silica: Evidence of the structural association of Al and Si in diatom frustules. *Geochim. Cosmochim. Acta* 66, 1601–1609. doi: 10.1016/S0016-7037(01)00877-8.
Gehlen, M., van Raaphorst, W., 1993. Early diagenesis of silica in sandy North sea sediments: quantification of the solid phase. *Mar. Chem.* 42, 71–83. doi: 10.1016/0304-4203(93)90238-J.
Grasshoff, K., Ehrhardt, M., Kremling, K., 1983. Methods of seawateranalysis. 2nd Edition Vol. 419 (Weinheim: WILEY-VCH Verlag Chemie GmbH).
Griffin, J. J., Windom, H., Goldberg, E. D., 1968. The distribution of clay minerals in the World Ocean. *Deep. Res. Oceanogr. Abstr.* 15, 433–459. doi: 10.1016/0011-7471(68)90051-X.
Huang, T. H., Sun, X., Somelar, P., Kirsimäe, K., Pickering, R. A., Kim, J. H., Kielman-Schmitt, M., Hong, W. L., 2023. Separating Si phases from diagenetically-modified sediments through sequential leaching. *Chem. Geol.* 637. doi: 10.1016/j.chemgeo.2023.121681.
Hurd, D. C., 1983. Physical and chemical properties of ciliceous skeletons, in: S. R. Aston (Eds.), *Silicon Geochemistry and Biogeochemistry*, Academic Press, London, pp. 187–245.
Hydes, D. J., Liss, P. S., 1976. Fluorimetric method for the determination of low concentrations of dissolved aluminium in natural waters. *Analyst* 101, 922–931. doi: 10.1039/an9760100922.
Jaijel, R., Goodman Tchernov, B. N., Biton, E., Weinstein, Y., Katz, T., 2021. Optimizing a standard preparation procedure for grain size analysis of marine sediments by laser diffraction (MS-PT4SD: Marine sediments-pretreatment for size distribution). *Deep. Res. Part I Oceanogr. Res. Pap.* 167. doi:

10.1016/j.dsr.2020.103429.
Jeandel, C., 2016. Overview of the mechanisms that could explain the "Boundary Exchange" at the land-ocean contact. *Philos. Trans. R. Soc. A Math. Phys. Eng. Sci.* 374. doi: 10.1098/rsta.2015.0287.
Jeandel, C., Oelkers, E. H., 2015. The influence of terrigenous particulate material dissolution on ocean chemistry and global element cycles. *Chem. Geol.* 395, 50–66. doi: 10.1016/j.chemgeo.2014.12.001.
Jeandel, C., Peucker-Ehrenbrink, B., Jones, M. T., Pearce, C. R., Oelkers, E. H., Godderis, Y., Lacan, F., Aumont, O., Arsouze, T., 2011. Ocean margins: The missing term in oceanic element budgets? *Eos,Transactions, American geophysical Union* 92, 217–218. doi: 10.1029/2011EO260001.
Kamatani, A., Oku, O., 2000. Measuring biogenic silica in marine sediments. *Mar. Chem.* 68, 219–229. doi: 10.1016/S0304-4203(99)00079-1.
Köhler, S. J., Bosbach, D., Oelkers, E. H., 2005. Do clay mineral dissolution rates reach steady state? *Geochim. Cosmochim. Acta* 69, 1997–2006. doi: 10.1016/j.gca.2004.10.015.
Koning, E., Epping, E., Van Raaphorst, W., 2002. Determining biogenic silica in marine samples by tracking silicate and aluminium concentrations in alkaline leaching solutions. *Aquat. Geochemistry* 8, 37–67. doi: 10.1023/A:1020318610178.
Koning, E., Gehlen, M., Flank, A. M., Calas, G., Epping, E., 2007. Rapid post-mortem incorporation of aluminum in diatom frustules: Evidence from chemical and structural analyses. *Mar. Chem.* 103, 97–111. doi: 10.1016/j.marchem.2006.09.001.
Krause, W., Darrow, E. S., Pickering, R. A., Carmichael, R. H., Larson, A. M., Basaldua, J. L., 2017. Reactive silica fractions in coastal lagoon sediments from the northern Gulf of Mexico. 151, 8–14. doi: 10.1016/j.csr.2017.09.014.
Lerman, A., Mackenzie, F. T., Bricker, O. P., 1975. Rate of Dissoution of Aluminosilicates in Seawater. *Earth Planet. Sci. Lett.* 25, 82–88. doi: 10.1016/0012-821X(75)90213-7.
Leynaert, A., Longphuirt, S. N., An, S., Lim, J. H., Claquin, P., Grall, J., Kwon, B. O., Koh, C. H., 2011. Tidal variability in benthic silicic acid fluxes and microphytobenthos uptake in intertidal sediment. *Estuar. Coast. Shelf Sci.* 95, 59–66. doi: 10.1016/j.ecss.2011.08.005.
Li, L., Li, F. M., Wang, Z. W., Zhao, M. X., Zhang, J., Ren, J. L., 2018. Factors influencing the use of dissolved aluminum as a source tracer in the East China Sea and adjacent waters. *Mar. Chem.* 204, 133–143. doi: 10.1016/j.marchem.2018.05.009.
Liao, W. H., Planquette, H., Moriceau, B., Lambert, C., Desprez de Gesincourt, F., Laurenceau-Cornec, E., Sarthou, G., Gorgues, T., 2023. The effect of temperature on the release of silicon, iron and manganese into seawater from resuspended sediment particles. *Geochim. Cosmochim. Acta* 351, 1–13. doi: 10.1016/j.gca.2023.04.014.
Liu, S. M., Hong, G. H., Zhang, J., Ye, X. W., Jiang, X. L., 2009. Nutrient budgets for

large Chinese estuaries. *Biogeosciences* 6, 2245–2263. doi: 10.5194/bg-6-2245-2009.

Liu, S. M., Li, L. W., Zhang, Z., 2011. Inventory of nutrients in the Bohai. *Cont. Shelf Res.* 31, 1790–1797. doi: 10.1016/j.csr.2011.08.004.

Liu, S. M., Zhang, J., Chen, S. Z., Chen, H. T., Hong, G. H., Wei, H., Wu, Q. M., 2003. Inventory of nutrient compounds in the Yellow Sea. *Cont. Shelf Res.* 23, 1161–1174. doi: 10.1016/S0278-4343(03)00089-X.

Liu, S. M., Zhang, J., Li, R. X., 2005. Ecological significance of biogenic silica in the East China Sea. *Mar. Ecol. Prog. Ser.* 290, 15–26. doi: 10.3354/meps290015.

Loucaides, S., Michalopoulos, P., Presti, M., Koning, E., Behrends, T., Van Cappellen, P., 2010. Seawater-mediated interactions between diatomaceous silica and terrigenous sediments: Results from long-term incubation experiments. *Chem. Geol.* 270, 68–79. doi: 10.1016/j.chemgeo.2009.11.006.

Ma, Y., Yang, B., Zhou, N., Huang, J., Liu, S. M., Zhu, D., Liang, W., 2023. Distribution and dissolution kinetics of biogenic silica in sediments of the northern South China Sea. *Front. Mar. Sci.* 10, 1–15. doi: 10.3389/fmars.2023.1083233.

Ma, Y., Zhang, L., Liu, S., and Zhu, D., 2022. Silicon balance in the South China Sea. *Biogeochemistry* 157, 327–353. doi: 10.1007/s10533-021-00879-4.

Mackenzie, F. T., Garrels, R. M., Bricker, O. P., Bickley, F., 1967. Silica in sea water: Control by silica minerals. *Science* 155, 1404–1405. doi: 10.1126/science.155.3768.1404.

Mackin, J. E., Aller, R. C., 1984. Dissolved Al in sediments and waters of the East China Sea: Implications for authigenic mineral formation. *Geochim. Cosmochim. Acta* 48, 281–297. doi: 10.1016/0016-7037(84)90251-5.

Maldonado, M., López-Acosta, M., Abalde, S., Martos, I., Ehrlich, H., Leynaert, A., 2022. On the dissolution of sponge silica: Assessing variability and biogeochemical implications. *Front. Mar. Sci.* 9, 1–16. doi: 10.3389/fmars.2022.1005068.

Measures, C. I., Hatta, M., 2021. On Using Si to Unravel Potential Sources of Dissolved Al to the Deep Arctic. *J. Geophys. Res. Ocean.* 126, 1–17. doi: 10.1029/2021JC017399.

Mei, X., Li, X., Mi, B., Zhao, L., Wang, Z., Zhong, H., Hao, Y., Huang, X., He, M., Zhang, Y., 2020. Distribution regularity and sedimentary differentiation patterns of China seas surface sediments. *Geol. China* 47, 1447–1462. doi: 10.12029/gc20200511.

Michalopoulos, P., Aller, R. C., 1995. Rapid clay mineral formation in Amazon delta sediments: Reverse weathering and oceanic elemental cycles. *Science (80-.).* 270, 614–617. doi: 10.1126/science.270.5236.614.

Michalopoulos, P., Aller, R. C., 2004. Early diagenesis of biogenic silica in the Amazon delta: Alteration, authigenic clay formation, and storage. *Geochim. Cosmochim. Acta* 68, 1061–1085. doi: 10.1016/j.gca.2003.07.018.

Michalopoulos, P., Aller, R. C., Reeder, R. J., 2000. Conversion of diatoms to clays during early diagenesis in tropical, continental shell muds. *Geology* 28, 1095–1098. doi: 10.1130/0091-7613(2000)028<1095:CODTCD>2.3.CO;2.

Milliman, J. D., Meade, R. H., 1983. World wide delivery of river sediments to oceans. *J. Geol.* 91, 1–21. doi: 10.1086/628741.

Moriceau, B., Goutx, M., Guigue, C., Lee, C., Armstrong, R., Duflos, M., Tamburini, C., Charriére., B., Ragueneau, O., 2009. Si-C interactions during degradation of the diatom Skeletonema marinoi. *Deep. Res. Part II Top. Stud. Oceanogr.* 56, 1381–1395. doi: 10.1016/j.dsr2.2008.11.026.

Mortlock, R. A., Froelich, P. N., 1989. A simple method for the rapid determination of biogenic opal in pelagic marine sediments. *Deep Sea Res. Part A, Oceanogr. Res. Pap.* 36, 1415–1426. doi: 10.1016/0198-0149(89)90092-7.

Ng, H. C., Cassarino, L., Pickering, R. A., Woodward, E. M. S., Hammond, S. J., Hendry, K. R., 2020. Sediment efflux of silicon on the Greenland margin and implications for the marine silicon cycle. *Earth Planet. Sci. Lett.* 529, 115877. doi: 10.1016/j.epsl.2019.115877.

Ng, H. C., Hawkings, J. R., Bertrand, S., Summers, B. A., Sieber, M., Conway, T. M., Freitas, F. S., Ward, J. P. J., Pryer, H. V., Wadham, J. L., Arndt, S., Hendry, K. R., 2022. Benthic Dissolved Silicon and Iron Cycling at Glaciated Patagonian Fjord Heads. *Global Biogeochem. Cycles* 36, 1–22. doi: 10.1029/2022GB007493.

Niibori, Y., Kunita, M., Tochiyama, O., Chida, T., 2000. Dissolution Rates of Amorphous Silica in Highly Alkaline Solution. *J. Nucl. Sci. Technol.* 37, 349–357. doi: 10.1080/18811248.2000.9714905.

Oehler, T., Schlüter, M., Schückel, U., 2015. Seasonal dynamics of the biogenic silica cycle in surface sediments of the Helgoland Mud Area (southern North Sea). *Cont. Shelf Res.* 107, 103–114. doi: 10.1016/j.csr.2015.07.016.

Oinuma, K., Kobayashi, K., 1966. Quantitative Study of Clay Minerals in Some Recent Marine Sediments and Sedimentary Rocks from Japan. *Clays Clay Miner.* 14, 209–219. doi: 10.1346/CCMN.1966.0140118.

Passow, U., 1991. Species-specific sedimentation and sinking velocities of diatoms. *Mar. Biol.* 108, 449–455. doi: 10.1007/BF01313655.

Petschick, R., 2002. MacDiff 4.2.6 (Version 4.2.6). http://servermac.geologie.uni-frankfurt.de/Rainer.html.

Phillips, A. K., 2020. Modelling riverine dissolved silica on different spatial and temporal scales using statistical and machine learning methods. [Dissertation]. University of Toronto. https://hdl.handle.net/1807/101210.

Pickering, R. A., Cassarino, L., Hendry, K. R., Wang, X. L., Maiti, K., Krause, J. W., 2020. Using Stable Isotopes to Disentangle Marine Sedimentary Signals in Reactive Silicon Pools. Geophys. Res. Lett. 47, 0–3. doi: 10.1029/2020GL087877.

Pickering, R. A., Wang, X. L., Hendry, K. R., Maiti, K., Krause, J. W., 2023. An investigation into the characteristics of reactive silicon pools of coastal marine sediments. Cont. Shelf Res. 268, 105126. doi: 10.1016/j.csr.2023.105126.

Qiao, S., Shi, X., Wang, G., Zhou, L., Hu, B., Hu, L., Yang, G., Liu, Y, Yao, Z., Liu, S., 2017. Sediment accumulation and budget in the Bohai Sea, Yellow Sea and East China Sea. *Mar. Geol.* 390, 270–281. doi: 10.1016/j.margeo.2017.06.004.

Qu, H., Xu, Y., Wang, J., Li, X. Z., 2020. Radiolarian assemblages in the shelf area of the East China Sea and Yellow Sea and their ecological indication of the Kuroshio

Current derivative branches. *PeerJ* 8, 1–19. doi: 10.7717/peerj.9976.
Raimonet, M., Ragueneau, O., Jacques, V., Corvaisier, R., Moriceau, B., Khripounoff, A., Pozzato, L., Rabouille, C., 2015. Rapid transport and high accumulation of amorphous silica in the Congo deep-sea fan: A preliminary budget. *J. Mar. Syst.* 141, 71–79. doi: 10.1016/j.jmarsys.2014.07.010.
Ran, L., Chen, J., Wiesner, M. G., Ling, Z., Lahajnar, N., Yang, Z., Li, H., Hao, Q., Wang, K., 2015. Variability in the abundance and species composition of diatoms in sinking particles in the northern South China Sea: Results from time-series moored sediment traps. *Deep. Res. Part II Top. Stud. Oceanogr.* 122, 15–24. doi: 10.1016/j.dsr2.2015.07.004.
Ran, X., Liu, J., Liu, S., Zang, J., Wang, B., Zhao, J., 2018. The biogenic silica composition, behavior and budget in the Changjiang Estuary. *Acta Oceanol. Sin.* 37, 60–72. doi: 10.1007/s13131-018-1159-7.
Rahman, S., Aller, R. C., Cochran, J. K., 2016. Cosmogenic ^{32}Si as a tracer of biogenic silica burial and diagenesis: Major deltaic sinks in the silica cycle. *Geophys. Res. Lett.* 43, 7124–7132. doi: 10.1002/2016GL069929.
Ren, H., Brunelle, B. G., Sigman, D. M., Robinson, R. S., 2013. Diagenetic aluminum uptake into diatom frustules and the preservation of diatom-bound organic nitrogen. *Mar. Chem.* 155, 92–101. doi: 10.1016/j.marchem.2013.05.016.
Ren, J. L., Zhang, J., Li, J. B., Yu, X. Y., Liu, S. M., Zhang, E. R., 2006. Dissolved aluminum in the Yellow Sea and East China Sea - Al as a tracer of Changjiang (Yangtze River) discharge and Kuroshio incursion. *Estuar. Coast. Shelf Sci.* 68, 165–174. doi: 10.1016/j.ecss.2006.02.004.
Rickert, D., 2000. Dissolution kinetics of biogenic silica in marine environments= Lösungskinetik von biogenem Opal in marinen Systemen. Reports on Polar Research, Alfred Wegener Institute for Polar and Marine Research. https://epic.awi.de/id/eprint/26530/1/BerPolarforsch2000351.pdf.
Rickert, D., Schlüter, M., Wallmann, K., 2002. Dissolution kinetics of biogenic silica from the water column to the sediments. *Geochim. Cosmochim. Acta* 66, 439–455. doi: 10.1016/S0016-7037(01)00757-8.
Schlitzer, Reiner, Ocean Data View, odv.awi.de, 2023. https://odv.awi.de/.
Shi X. F., Liu Y. G., Qiao S. Q., Liu S. F., Wang K. S., 2021. Sediment type map of the Bohai Sea, Yellow Sea and East China Sea, First ed. Science Press, Beijing.
Siever, R., 1968. Establishment of equilibrium between clays and sea water. *Earth Planet. Sci. Lett.* 5, 106–110. doi: 10.1016/S0012-821X(68)80023-8.
Sutton, J. N., André, L., Cardinal, D., Conley, D. J., De Souza, G. F., Dean, J., Dodd, J., Ehlert, C., Ellwood, M. J., Frings, P. J., Grasse, P., Hendry, K., Leng, M. J., Michalopoulos, P., Panizzo, V. N., Swann, G. E. A., 2018. A review of the stable isotope bio-geochemistry of the global silicon cycle and its associated trace elements. *Front. Earth Sci.* 5. doi: 10.3389/feart.2017.00112.
Taucher, J., Bach, L. T., Prowe, A. E. F., Boxhammer, T., Kvale, K., Riebesell, U., 2022. Enhanced silica export in a future ocean triggers global diatom decline. *Nature* 605, 696–700. doi: 10.1038/s41586-022-04687-0.
Tréguer, P., Bowler, C., Moriceau, B., Dutkiewicz, S., Gehlen, M., Aumont, O., Bittner,

L., Dugdale, R., Finkel, Z., Iudicone, D., Jahn, O., Guidi, L., Lasbleiz, M., Leblanc, K., Levy, M., Pondaven, P., 2018. Influence of diatom diversity on the ocean biological carbon pump. *Nat. Geosci.* 11, 27–37. doi: 10.1038/s41561-017-0028-x.

Tréguer, P., Nelson, D. M., Van Bennekom, A. J., DeMaster, D. J., Leynaert, A., Quéguiner, B., 1995. The silica balance in the world ocean: A reestimate. *Science* 268, 375–379. doi: 10.1126/science.268.5209.375.

Tréguer, P., Sutton, J., Brzezinski, M., Charette, M., Devries, T., Dutkiewicz, S., Ehlert, C., Hawkings, J., Leynaert, A., Liu, S. M., Monferrer, L. N., López-Acosta, M., Maldonado, M., Rahman, S., Ran, L., Rouxel, O., 2021. Reviews and syntheses: The biogeochemical cycle of silicon in the modern ocean. *Biogeosciences Discuss.* 18, 1269–1289. doi: 10.5194/bg-2020-274.

van Bennekom, A. J., Fred Jansen, J. H., van der Gaast, S. J., van Iperen, J. M., Pieters, J., 1989. Aluminium-rich opal: an intermediate in the preservation of biogenic silica in the Zaire (Congo) deep-sea fan. *Deep Sea Res. Part A, Oceanogr. Res. Pap.* 36, 173–190. doi: 10.1016/0198-0149(89)90132-5.

Van Beusekom, J. E. E., Van Bennekom, A. J., Tréguer, P., Morvan, J., 1997. Aluminium and silicic acid in water and sediments of the Enderby and Crozet Basins. *Deep. Res. Part II Top. Stud. Oceanogr.* 44, 987–1003. doi: 10.1016/S0967-0645(96)00105-1.

Van Cappellen, P., Dixit, S., van Beusekom, J., 2002. Biogenic silica dissolution in the oceans: Reconciling experimental and field-based dissolution rates. *Global Biogeochem. Cycles* 16, 23-1-23–10. doi: 10.1029/2001gb001431.

Van Cappellen, P., Qiu, L., 1997. Biogenic silica dissolution in sediments of the Southern Ocean. I. Solubility. *Deep. Res. Part II Top. Stud. Oceanogr.* 44, 1109–1128. doi: 10.1016/S0967-0645(96)00113-0.

Ward, J. P. J., Hendry, K. R., Arndt, S., Faust, J. C., Freitas, F. S., Henley, S. F., Krause, J. F., Marz, C., Ng, C. H., Pickering, R. A., Tessin, A. C., 2022. Stable silicon isotopes uncover a mineralogical control on the benthic silicon cycle in the Arctic Barents Sea. *Geochim. Cosmochim. Acta* 329, 206–230. doi: 10.1016/j.gca.2022.05.005.

Wang, L., Fan, D., Li, W., Liao, Y., Zhang, X., Liu, M., Yang, Z., 2014. Grain-size effect of biogenic silica in the surface sediments of the East China Sea. *Cont. Shelf Res.* 81, 29–37. doi: 10.1016/j.csr.2014.03.005.

Wentworth, C.K., 1922. A scale of grade and class terms for clastic sediments. Journal of Geology 30, 377–392.

Wu, B., Liu, S., 2020. Dissolution kinetics of biogenic silica and the recalculated silicon balance of the East China Sea. *Sci. Total Environ.* 743, 140552. doi: 10.1016/j.scitotenv.2020.140552.

Wu, B., Liu, S. M., Ren, J. L., 2017. Dissolution kinetics of biogenic silica and tentative silicon balance in the Yellow Sea. *Limnol. Oceanogr.* 62, 1512–1525. doi: 10.1002/lno.10514.

Wu Z.Y. Wen Z.H., 2019. Marine Geology Map of the China Sea Series. First ed. Science Press, Beijing.

916 Zhang, L., Wang, R., Chen, M., Liu, J., Zeng, L., Xiang, R., Zhang, Q., 2015. Biogenic
917 silica in surface sediments of the South China Sea: Controlling factors and
918 paleoenvironmental implications. *Deep. Res. Part II Top. Stud. Oceanogr.* 122,
919 142–152. doi: 10.1016/j.dsr2.2015.11.008.
920 Zhang, X., Ren, J., Guo, Y., Lei, L., Zhang, R., 2020. Distributions and influencing
921 factors of dissolved aluminum in the Zhujiang River Estuary,con- tinental slope
922 of the northern South China Sea in autumn and summer. *Haiyang Xuebao* 42, 10–
923 20. doi: 10.3969/j.issn.0253− 4193.2020.02.002.
924 Zhang, Z., Sun, X., Dai, M., Cao, Z., Fontorbe, G., Conley, D. J., 2020. Impact of
925 human disturbance on the biogeochemical silicon cycle in a coastal sea revealed
926 by silicon isotopes. Limnol. Oceanogr. 65, 515–528. doi: 10.1002/lno.11320.
927 Zhu, D., Sutton, J. N., Leynaert, A., Tréguer, P. J., Schoelynck, J., Gallinari, M., Ma,
928 Y., Liu, S. M., 2023. Revisiting the biogenic silica burial flux determinations: A
929 case study for the East China seas. *Front. Mar. Sci.* 9, 1–22. doi:
930 10.3389/fmars.2022.1058730.
931

Appendix A.

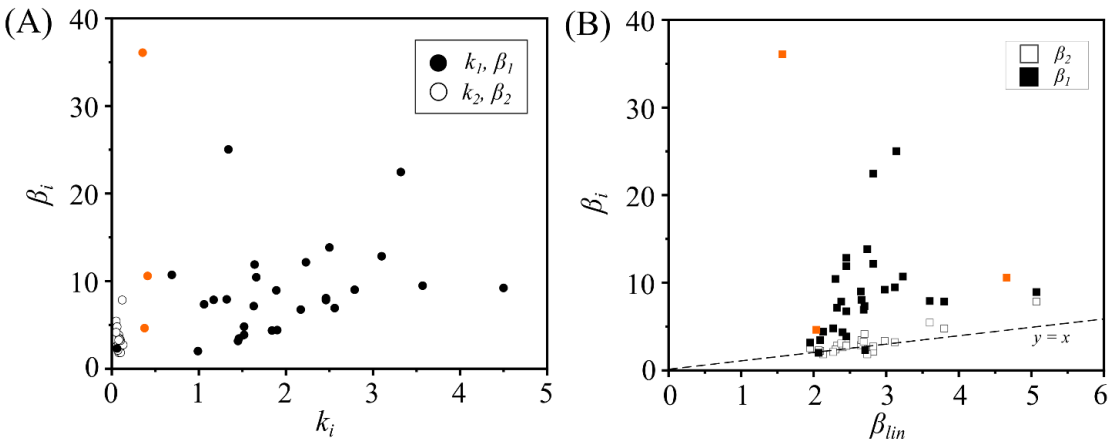

Figure A1. Relationsip of A): reactivity (k_i) of non-linear dissolving Si fraction and Si:Al ratios (β_i) and B) the Si:Al ratio of lSi (β_{lin}) and non-linear dissolving Si fractions (β_i). The symbols in orange represents samples of Northern South China Sea (NSCS) that contain one non-linear dissolving Si fraction.

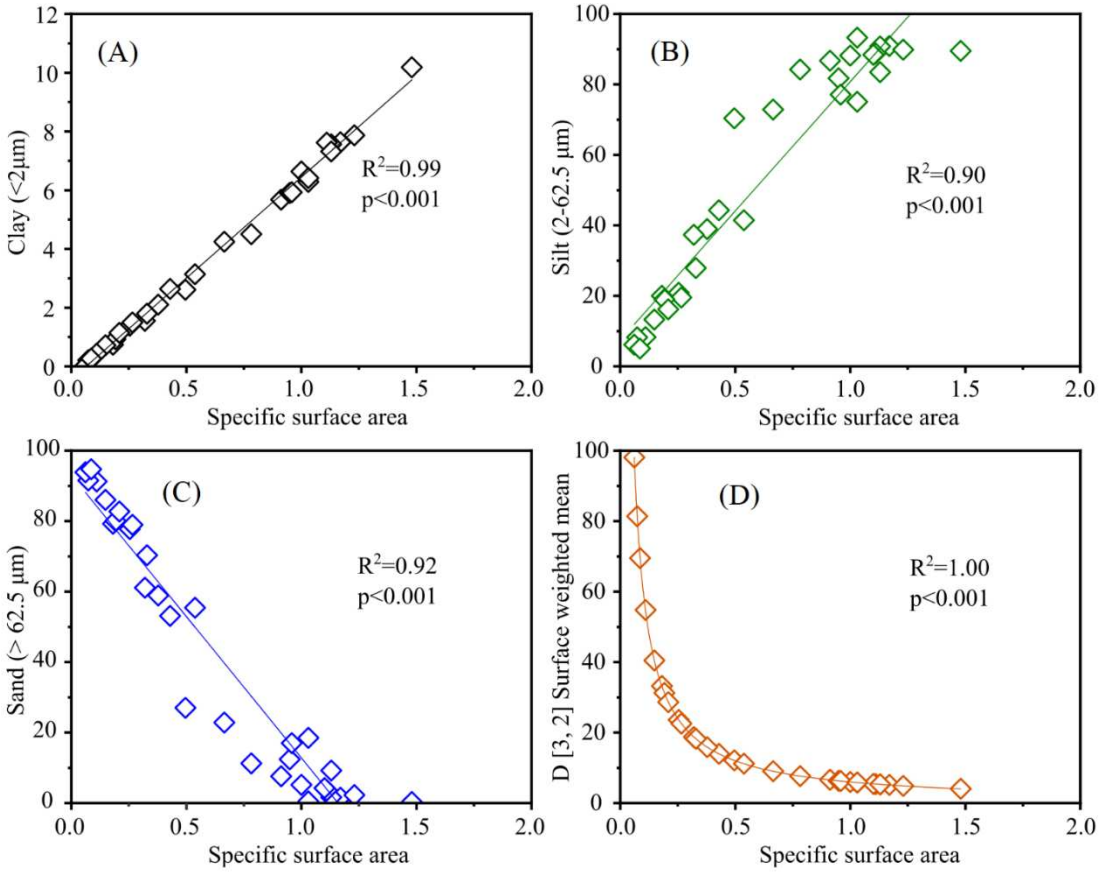

938

939 **Figure A2.** Plot of calculated specific surface area (SSA) of sediment and grain-size.

940 (A) SSA vs. Clay%, (B) SSA vs. Silt%, (C) SSA vs. Sand%, and (D) SSA vs. D [3, 2]

941 surface weighted mean.

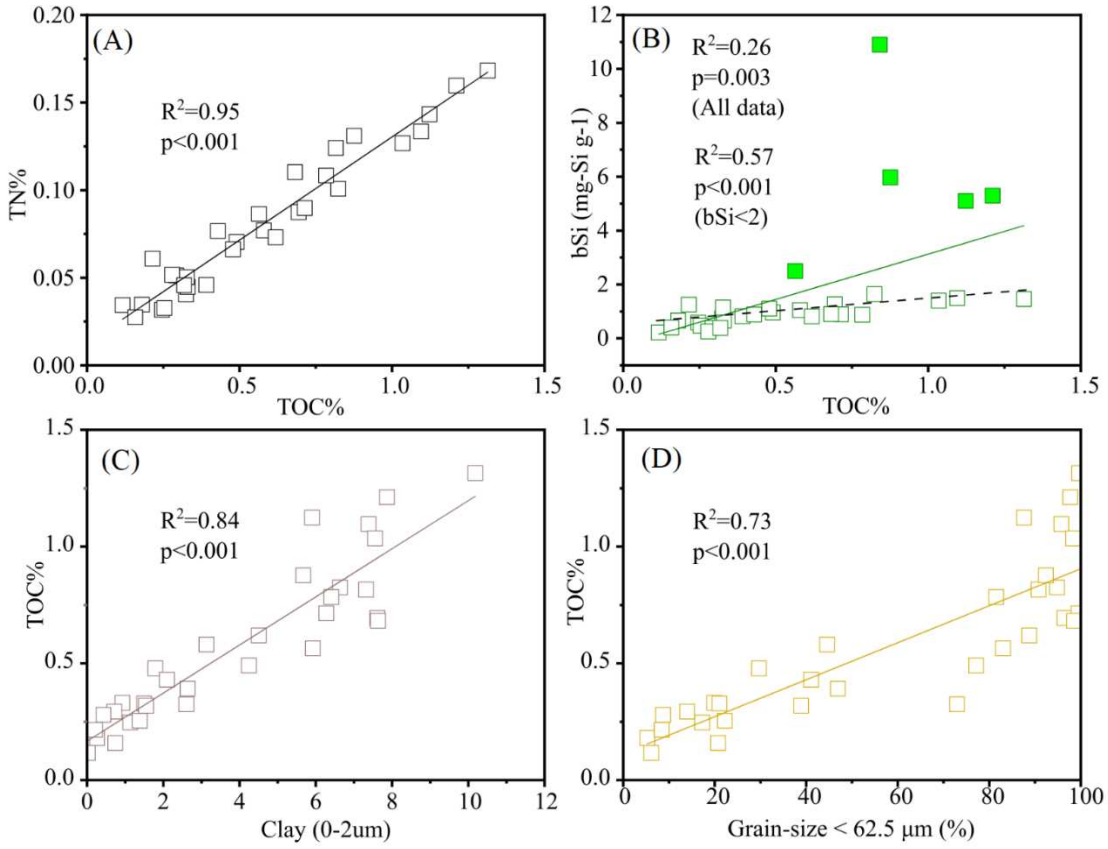

Figure A3. Different sediment chemical compositions and their relationship with grain-size. The squares filled in green color (see plot B) represent samples from the continental slope of ECS (C12, D12, DC and F8) and SCS (NSCS7).

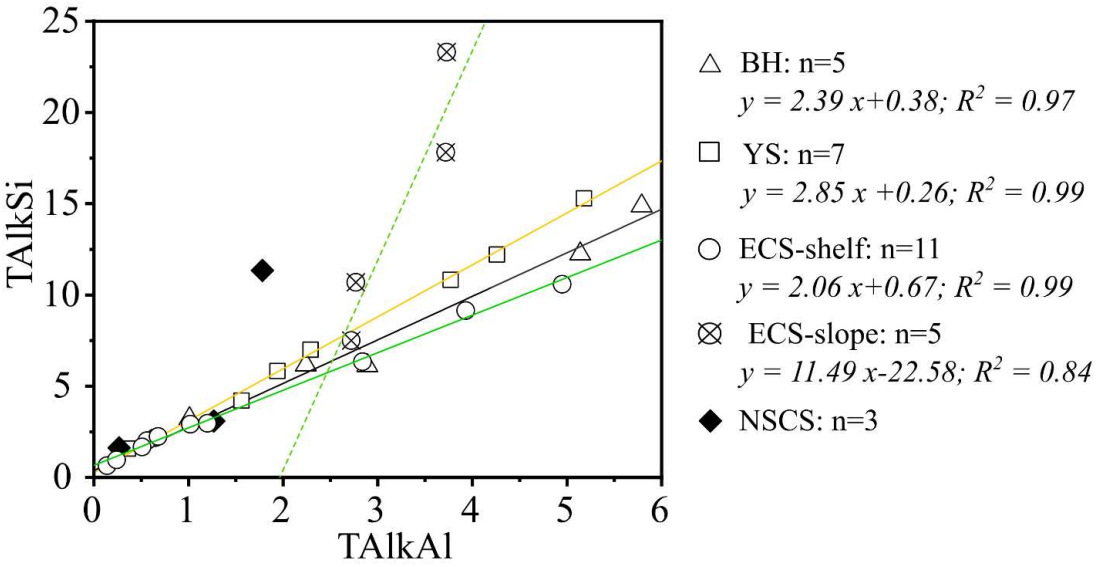

946

947 **Figure A4.** Total amount of alkaline extracted Si (TAlkSi, mg-Si g^{-1})and Al (TAlkAl,
948 mg-Al g^{-1}). The lines in black, yellow, green color are linear fitted data of samples from
949 BH, YS and ECS. The dashed green line represent fitted data of samples obtained from
950 ECS slope. Filled symbles represent NSCS samples.